An affinity-directed phosphatase, AdPhosphatase, system for targeted protein dephosphorylation

Simpson, Luke M.; Fulcher, Luke J.; Sathe, Gajanan; Brewer, Abigail; Zhao, Jin-Feng; Squair, Daniel R.

Published in:
Cell Chemical Biology

DOI:
10.1016/j.chembiol.2023.01.003

Publication date:
2023

Article

Cell Chemical Biology

An affinity-directed phosphatase, AdPhosphatase, system for targeted protein dephosphorylation

Graphical abstract

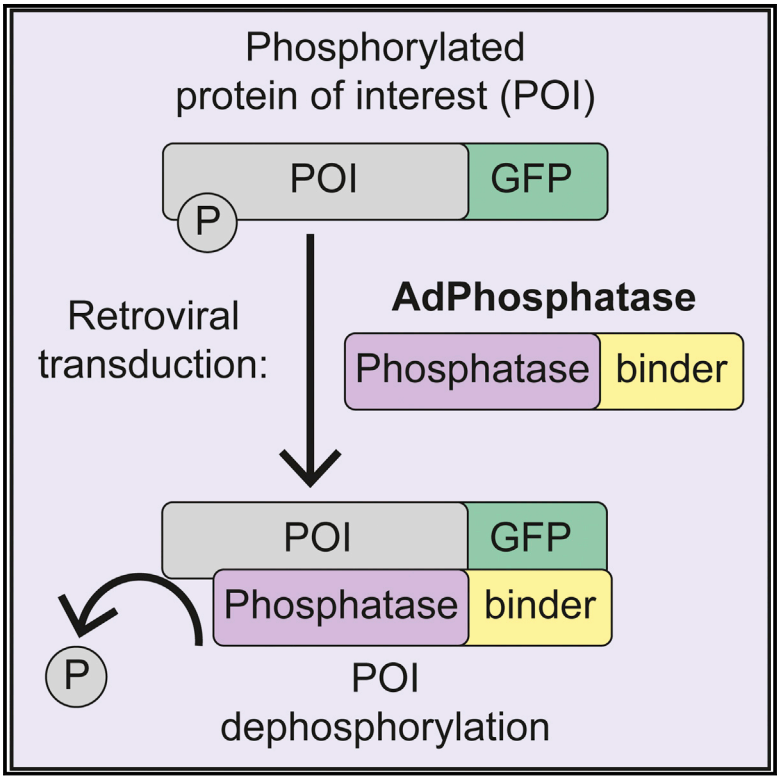

Authors

Luke M. Simpson, Luke J. Fulcher, Gajanan Sathe, ..., Joby Varghese, Renata F. Soares, Gopal P. Sapkota

Correspondence

g.sapkota@dundee.ac.uk

In brief

Simpson and Fulcher et al. describe the development of an affinity-directed phosphatase (AdPhosphatase) system to promote targeted dephosphorylation of phosphorylated proteins of interest (POIs). The AdPhosphatase consists of a POI-binding nanobody conjugated to the catalytic subunit of a promiscuous phosphatase (PPP1CA/PPP2CA), which can mediate POI dephosphorylation through proximity in cells.

Highlights

- Affinity-directed phosphatase (AdPhosphatase) can mediate protein dephosphorylation
- AdPhosphatase consists of a target binder conjugated to a phosphatase catalytic subunit
- Target dephosphorylation by AdPhosphatase requires phosphatase catalytic activity
- AdPhosphatase system can be used to study the role of target protein phosphorylation

Simpson et al., 2023, Cell Chemical Biology *30*, 188–202
February 16, 2023
https://doi.org/10.1016/j.chembiol.2023.01.003

CellPress

CellPress
OPEN ACCESS

Cell Chemical Biology

Article

An affinity-directed phosphatase, AdPhosphatase, system for targeted protein dephosphorylation

Luke M. Simpson,[1,3] Luke J. Fulcher,[1,2,3] Gajanan Sathe,[1] Abigail Brewer,[1] Jin-Feng Zhao,[1] Daniel R. Squair,[1] Jennifer Crooks,[1] Melanie Wightman,[1] Nicola T. Wood,[1] Robert Gourlay,[1] Joby Varghese,[1] Renata F. Soares,[1] and Gopal P. Sapkota[1,4,*]

[1]Medical Research Council (MRC) Protein Phosphorylation and Ubiquitylation Unit, School of Life Sciences, University of Dundee, Dundee DD1 5EH, UK

[2]Present address: Department of Biochemistry, University of Oxford, South Parks Road, Oxford OX1 3QU, UK

[3]These authors contributed equally

[4]Lead contact

*Correspondence: g.sapkota@dundee.ac.uk

https://doi.org/10.1016/j.chembiol.2023.01.003

SUMMARY

Reversible protein phosphorylation, catalyzed by protein kinases and phosphatases, is a fundamental process that controls protein function and intracellular signaling. Failure of phospho-control accounts for many human diseases. While a kinase phosphorylates multiple substrates, a substrate is often phosphorylated by multiple kinases. This renders phospho-control at the substrate level challenging, as it requires inhibition of multiple kinases, which would thus affect other kinase substrates. Here, we describe the development and application of the affinity-directed phosphatase (AdPhosphatase) system for targeted dephosphorylation of specific phospho-substrates. By deploying the Protein Phosphatase 1 or 2A catalytic subunits conjugated to an antigen-stabilized anti-GFP nanobody, we can promote the dephosphorylation of two independent phospho-proteins, FAM83D or ULK1, knocked in with GFP-tags using CRISPR-Cas9, with exquisite specificity. By redirecting protein phosphatases to neo-substrates through nanobody-mediated proximity, AdPhosphatase can alter the phospho-status and function of target proteins and thus, offers a new modality for potential drug discovery approaches.

INTRODUCTION

Protein phosphorylation is a reversible post-translation modification (PTM) characterized by the covalent addition of a phosphate group to primarily serine, threonine, or tyrosine residues on the surface of a protein.[1,2] Protein phosphorylation is catalyzed by protein kinases, while protein phosphatases mediate the reverse reaction by hydrolyzing the phosphorylated amino acid residue.[3] The phosphorylation status of a protein can alter its function through potentially several avenues: modulating its enzymatic activity, folding, stability, subcellular localization, and/or by influencing its protein-protein interactions.[4] Almost all aspects of mammalian cell biology are regulated by reversible protein phosphorylation, with abnormal phosphorylation being identified as the cause of a wide range of human pathologies, including many cancers and neurodegenerative diseases.[2,5] Therefore, significant research efforts have strived to develop specific protein kinase inhibitors and activators for use in both therapeutics and for studying cell signaling processes, albeit progress with phosphatases has been more limited.[6–8] However, even highly selective protein kinase inhibitors suffer from the fact that they block phosphorylation of all the downstream substrates of the inhibited kinase, rendering inhibition of specific substrate phosphorylation events very challenging. Furthermore, both kinase and phosphatase inhibitors are often known to elicit off-target effects.[7–17] To study substrate-level phospho-control in cells, mutations of phospho-residues to either block phosphorylation (e.g., Ala or Val substitutions) or mimic phosphorylation (negatively charged Asp or Glu substitutions) are common, but these mutations have the potential to alter protein conformation, especially if there are multiple phospho-residues to be mutated, whereas phospho-mimetics are chemically distinct[18] and do not always mimic true phosphorylation state.[19] Amber stop-codon engineering to allow for site-specific incorporation of phospho-residues[20] can directly overcome problems associated with mimetic mutations, but this technology requires complex genetic manipulation of target cells and does not work for every phospho-residue or protein. In contrast, targeted dephosphorylation of a specific phosphorylated protein of interest (phospho-POI) by redirecting a catalytically active phosphatase to a desired neo-substrate has the potential to achieve exquisite substrate-level phospho-control. This approach would have the added benefit of also allowing dephosphorylation of phospho-substrates that may be phosphorylated by multiple upstream kinases, while not affecting the phospho-status of the other non-related substrates of those individual kinases.

It is estimated that 98% of phosphorylated residues in the human proteome are serine or threonine and a majority of these sites are dephosphorylated by just two ubiquitously expressed enzymes: protein phosphatase 1 (PP1) and protein phosphatase 2A (PP2A).[21,22] These enzymes, which are two of the most highly conserved proteins in eukaryotes, function within holoenzyme complexes that contain regulatory subunits that function to direct the catalytic subunits toward specific substrates.[21,23–25] Many regulatory subunits exist to mediate substrate specificity, including at least 200 known PP1 regulators and four classes of PP2A regulators (B/B55, B'/B56, B''/PR72 and Striatin), with multiple alternatively spliced isoforms evident for each class.[21] Whereas PP1 regulators bind directly to the catalytic domain via short linear motifs (SLiMs), most commonly via an RVxF consensus sequence, the PP2A regulatory subunits assemble with catalytic and scaffolding subunits into a heterotrimeric holoenzyme complex.[21,26,27] In the case of the PP2A-B56 class, the B56 regulatory subunit then binds directly to SLiMs to target this holoenzyme complex to specific substrates.[21]

To develop a system for targeted dephosphorylation, we conceptualized an affinity-directed system whereby we would artificially recruit the catalytic subunits of PP1 (PPP1CA) or PP2A (PPP2CA)[23–25] to distinct phospho-POIs via POI-specific polypeptide binders. We term this approach the affinity-directed phosphatase (AdPhosphatase). To test this concept, we focused on two distinct phospho-POIs: family with sequence similarity 83 member D (FAM83D) and the unc-51-like kinase 1 (ULK1). FAM83D is required for the recruitment of casein kinase 1α (CK1α) to the mitotic spindle to orchestrate proper spindle positioning and timely cell division.[28] During mitosis, FAM83D is heavily phosphorylated at the mitotic spindle in a CK1α-dependent manner, and is subsequently degraded by the proteasome upon mitotic exit.[28] However, the precise role for CK1α-dependent hyperphosphorylation of FAM83D remains elusive. The mitotic phosphorylation of FAM83D results in an electrophoretic mobility shift of approximately 25 kDa when visualized by immunoblotting, which can be collapsed by subjecting extracts to an *in vitro* dephosphorylation assay using λ-phosphatase.[28] As such, in the absence of phospho-specific antibodies, FAM83D immunoblots can be reliably used to monitor the phosphorylation status of FAM83D. ULK1 is a serine/threonine protein kinase that functions in a complex with both the autophagy-related protein 13 (ATG13) and the focal adhesion kinase family interacting protein of 200 kDa (FIP200) to regulate the initiation of autophagy.[29–31] In this capacity, ULK1 undergoes an intricate and diverse set of PTMs, including phosphorylation by different protein kinases at multiple residues, which can either activate or inhibit ULK1 kinase activity.[32]

For both FAM83D and ULK1, we previously generated and characterized cells harboring a GFP tag knocked into their endogenous loci using CRISPR-Cas9 genome editing technology: *FAM83D*$^{GFP/GFP}$ U2OS cells[28] and *ULK1*$^{GFP/GFP}$ ARPE-19 cells.[33] An AdPhosphatase construct was designed to harbor either PPP1CA or PPP2CA conjugated to an antigen-stabilized anti-GFP nanobody (aGFP$_{6M}$)[33,34] fused to a FLAG tag reporter (Figures 1A and 3A). aGFP$_{6M}$ is only stable when bound to its GFP target but is destabilized and degraded when unbound. Due to this property, homeostatic FLAG-aGFP$_{6M}$-PPP1CA/-PPP2CA levels close to a 1:1 ratio with the target POI-GFP would be expected to be maintained. A key advantage of this approach would therefore be to limit the overexpression of the AdPhosphatase and thereby avoid potential off-target dephosphorylation.[35,36] Encouragingly, following the expression of FLAG-aGFP$_{6M}$-PPP2CA in *FAM83D*$^{GFP/GFP}$ U2OS and *ULK1*$^{GFP/GFP}$ ARPE-19 cells, the levels of FLAG-aGFP$_{6M}$-PPP2CA are much lower than endogenous PPP2CA when detected using an anti-PPP2CA antibody (Figures S1A and S1B). Armed with the knowledge that aGFP$_{6M}$ was functioning to limit AdPhosphatase levels as intended, we sought to test the ability of these AdPhosphatases to target the dephosphorylation of phospho-FAM83D-GFP and phospho-ULK1-GFP and investigate the downstream biology.

RESULTS

Nanobody-directed recruitment of PPP1CA or PPP2CA mediates dephosphorylation of mitotic phospho-FAM83D-GFP

FAM83D directs CK1α to the mitotic spindle to ensure proper spindle positioning and timely cell division.[28] During mitosis, FAM83D also undergoes CK1α-dependent hyperphosphorylation, resulting in an ~25 kDa phospho-dependent electrophoretic mobility shift.[28] We postulated that upon expression of the FLAG-aGFP$_{6M}$-PPP1CA or -PPP2CA AdPhosphatases in *FAM83D*$^{GFP/GFP}$ knockin U2OS cells,[28] but not in wild-type (WT) cells, the phosphatase activity would be directed toward FAM83D-GFP and either mediate the dephosphorylation of hyper-phosphorylated FAM83D-GFP in mitosis or prevent FAM83D-GFP phosphorylation during mitosis (Figure 1A).

U2OS WT and *FAM83D*$^{GFP/GFP}$ cells transduced with retroviruses encoding FLAG-empty control, FLAG-aGFP$_{6M}$-PPP1CA, or FLAG-aGFP$_{6M}$-PPP2CA were synchronized in mitosis using the Eg5 inhibitor S-trityl-L-cysteine (STLC)[28] and FAM83D protein levels were analyzed (Figure 1B). In mitotic U2OS WT cells expressing FLAG-empty control, FLAG-aGFP$_{6M}$-PPP1CA or FLAG-aGFP$_{6M}$-PPP2CA, FAM83D phosphorylation was observed by the striking ~25 kDa electrophoretic mobility shift compared with asynchronous controls. These data suggest that the low levels of expression of FLAG-aGFP$_{6M}$-PPP1CA or FLAG-aGFP$_{6M}$-PPP2CA alone in cells do not interfere with the native untagged FAM83D phosphorylation during mitosis. In *FAM83D*$^{GFP/GFP}$ cells expressing FLAG-aGFP$_{6M}$-PPP1CA or FLAG-aGFP$_{6M}$-PPP2CA, but not those expressing FLAG-empty control, the mitotic phospho-FAM83D-GFP electrophoretic mobility shift collapsed, suggesting that targeted dephosphorylation of mitotic phospho-FAM83D-GFP was potentially achieved by both FLAG-aGFP$_{6M}$-PPP1CA and FLAG-aGFP$_{6M}$-PPP2CA AdPhosphatases.

To determine that phospho-FAM83D-GFP dephosphorylation is mediated through an interaction with FLAG-aGFP$_{6M}$-PPP1CA or FLAG-aGFP$_{6M}$-PPP2CA, extracts from both asynchronous and mitotic U2OS *FAM83D*$^{GFP/GFP}$ cells expressing FLAG-empty, FLAG-aGFP$_{6M}$-PPP1CA, or FLAG-aGFP$_{6M}$-PPP2CA were subjected to anti-GFP immunoprecipitation (IP) (Figure 1C). In both asynchronous and mitotic extracts, FLAG-aGFP$_{6M}$-PPP1CA or FLAG-aGFP$_{6M}$-PPP2CA co-precipitated with FAM83D-GFP. In addition, both CK1α and the microtubule-associated protein hyaluronan-mediated motility receptor

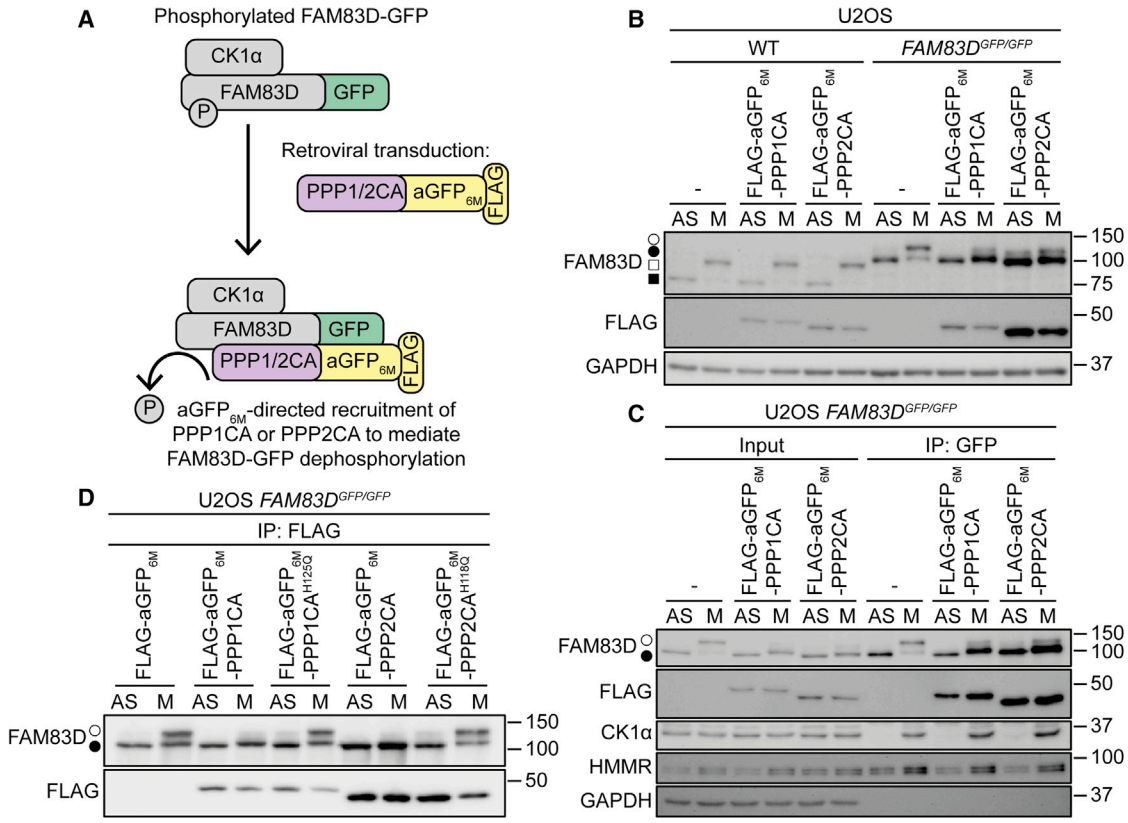

Figure 1. Anti-GFP nanobody-directed recruitment of PPP1CA or PPP2CA mediates dephosphorylation of mitotic phospho-FAM83D-GFP

(A) Schematic representation of anti-GFP nanobody ($aGFP_{6M}$)-directed recruitment of either PPP1CA or PPP2CA to GFP-tagged FAM83D to mediate FAM83D-GFP dephosphorylation.

(B) Wild-type (WT) and *FAM83D*$^{GFP/GFP}$ U2OS cells expressing FLAG-empty, FLAG-$aGFP_{6M}$-PPP1CA, or FLAG-$aGFP_{6M}$-PPP2CA were synchronized in mitosis using the Eg5 inhibitor S-trityl-L-cysteine (STLC) (5 μM) for 16 h. Following incubation, mitotic (M) cells were isolated through shake-off. Asynchronous (AS) cells were included as a control.

(C) U2OS *FAM83D*$^{GFP/GFP}$ FLAG-empty, FLAG-$aGFP_{6M}$-PPP1CA, or FLAG-$aGFP_{6M}$-PPP2CA-expressing cells were synchronized in mitosis using STLC, and M cells were isolated through shake-off. AS cells were included as a control. Cells were washed twice with ice-cold PBS, lysed, and subjected to anti-GFP immunoprecipitation (IP).

(D) U2OS *FAM83D*$^{GFP/GFP}$ FLAG-$aGFP_{6M}$, FLAG-$aGFP_{6M}$-PPP1CA, FLAG-$aGFP_{6M}$-PPP1CA^{H125Q}, FLAG-$aGFP_{6M}$-PPP2CA, or FLAG-$aGFP_{6M}$-PPP2CA^{H118Q} expressing cells were synchronized in mitosis using STLC, and M cells were isolated through shake-off. AS cells were included as a control. Cells were washed twice with ice-cold PBS, lysed, and subjected to anti-FLAG IP. For (B–D), extracts and/or IPs were resolved by SDS-PAGE and transferred on to PVDF membranes, which were subjected to immunoblotting with indicated antibodies. Closed square denotes AS endogenous FAM83D, open square denotes M endogenous FAM83D, closed circle denotes AS FAM83D-GFP, open circle denotes M FAM83D-GFP.

(HMMR, also referred to as RHAMM or CD168), which are validated endogenous FAM83D mitotic interactors,[28] co-precipitated with FAM83D-GFP from mitotic extracts from cells expressing FLAG-empty, FLAG-$aGFP_{6M}$-PPP1CA, or FLAG-$aGFP_{6M}$-PPP2CA, suggesting that FLAG-$aGFP_{6M}$-PPP1CA or FLAG-$aGFP_{6M}$-PPP2CA does not interfere with the endogenous FAM83D-CK1α-HMMR mitotic interactions. These data suggest that FLAG-$aGFP_{6M}$-PPP1CA or FLAG-$aGFP_{6M}$-PPP2CA interact with FAM83D-GFP to mediate the reduction in mitotic phosphorylation of phospho-FAM83D-GFP, and furthermore, their binding to FAM83D-GFP does not appear to interfere with native FAM83D interacting proteins.

To establish if the reduction in mitotic phosphorylation of phospho-FAM83D-GFP is reliant on the catalytic activity of PPP1CA or PPP2CA, asynchronous and mitotic U2OS *FAM83D*$^{GFP/GFP}$ cells expressing FLAG-empty, FLAG-$aGFP_{6M}$-PPP1CA, or FLAG-$aGFP_{6M}$-PPP2CA were treated with the protein phosphatase inhibitor Calyculin A (Cal A)[37,38] (Figure S2A). An increase in Akt S473 phosphorylation was observed upon Cal A treatment compared with DMSO-treated controls in all cells, suggesting effective protein phosphatase inhibition. Under these conditions, Cal A treatment caused similar FAM83D-GFP mobility shifts in asynchronous cells regardless of FLAG-empty, FLAG-$aGFP_{6M}$-PPP1CA, or FLAG-$aGFP_{6M}$-PPP2CA expression. The phospho-FAM83D-GFP electrophoretic mobility shift observed in mitotic DMSO-treated FLAG-empty control cells was shifted further upward by Cal A treatment. However, the mitotic phospho-FAM83D-GFP mobility shift in *FAM83D*$^{GFP/GFP}$ control cells that collapsed upon the expression of FLAG-$aGFP_{6M}$-PPP1CA or FLAG-$aGFP_{6M}$-PPP2CA did not fully restore with Cal A treatment, suggesting perhaps that the kinases that would be

expected to phosphorylate FAM83D in mitosis to cause the upward mobility shift did not do so over the course of Cal A treatment. The data were therefore inconclusive to establish that the dephosphorylation of phospho-FAM83D-GFP in mitosis is reliant on the phosphatase activity of FLAG-aGFP$_{6M}$-PPP1CA or FLAG-aGFP$_{6M}$-PPP2CA. Therefore, to definitively establish that targeted dephosphorylation is facilitated by the phosphatase activity of the AdPhosphatases, FLAG-aGFP$_{6M}$ empty and WT or catalytically dead AdPhosphatases (FLAG-aGFP$_{6M}$-PPP1CA/-PPP1CA^{H125Q} or FLAG-aGFP$_{6M}$-PPP2CA/-PPP2CA^{H118Q}, respectively)[24,39,40] were expressed in *FAM83D*$^{GFP/GFP}$ cells by retroviral transduction (Figure 1D). Asynchronous or mitotic extracts from these cells were then subjected to anti-FLAG IPs to only isolate pools of FAM83D-GFP exclusively bound to FLAG-aGFP$_{6M}$ or FLAG-aGFP$_{6M}$-linked to either WT or catalytically dead mutants of PPP1CA or PPP2CA (Figure 1D). A robust and complete collapse of the mitotic phospho-FAM83D-GFP electrophoretic mobility shift was observed in anti-FLAG-IPs from mitotic extracts from *FAM83D*$^{GFP/GFP}$ cells expressing either FLAG-aGFP$_{6M}$-PPP1CA or FLAG-aGFP$_{6M}$-PPP2CA compared with FLAG-aGFP$_{6M}$ controls, while no substantial mitotic phospho-FAM83D-GFP electrophoretic mobility shift was evident in anti-FLAG-IPs from mitotic extracts from cells expressing FLAG-aGFP$_{6M}$-PPP1CA^{H125Q} or FLAG-aGFP$_{6M}$-PPP2CA^{H118Q} catalytically dead mutants relative to FLAG-aGFP$_{6M}$ controls. These data establish that mitotic phospho-FAM83D-GFP dephosphorylation is reliant on the catalytic activity of the aGFP$_{6M}$-directed recruitment of PPP1CA or PPP2CA.

AdPhosphatase-mediated dephosphorylation of mitotic phospho-FAM83D prevents degradation of FAM83D

Previously, it has been shown that following CK1α-dependent phosphorylation of FAM83D at the mitotic spindle, FAM83D is subsequently degraded by the proteasome after mitotic exit,[28] although whether phosphorylation of FAM83D is required for its subsequent degradation is not known. To determine the effects of AdPhosphatase-mediated dephosphorylation of mitotic phospho-FAM83D-GFP on FAM83D-GFP protein stability following STLC release, U2OS *FAM83D*$^{GFP/GFP}$ cells expressing FLAG-empty, FLAG-aGFP$_{6M}$-PPP1CA (Figure 2A), FLAG-aGFP$_{6M}$-PPP1CA^{H125Q} (Figure 2A), FLAG-aGFP$_{6M}$-PPP2CA (Figure 2B), or FLAG-aGFP$_{6M}$-PPP2CA^{H118Q} (Figure 2B) were synchronized in mitosis using STLC and lysed at various time points following STLC washout. Following STLC release, as expected, a reduction in Cyclin B1,[41] HMMR, and phosphorylated FAM83D-GFP[28] levels can be observed 3–6 h after STLC washout in DMSO-treated FLAG-empty expressing control cells. In MG132-treated FLAG-empty control cells, an increase in polyubiquitylated substrates (Ub) was observed 3–6 h after STLC washout compared with DMSO-treated controls, suggesting successful inhibition of the proteasome. Under these conditions, phospho-FAM83D and HMMR were stabilised, as STLC-washout cells were unable to progress past metaphase due to proteasome inhibition preventing proteolysis of Cyclin B1 (Figure 2A) and Securin. These observations are consistent with previous data showing phospho-FAM83D and HMMR are degraded following mitotic exit.[29] In cells expressing FLAG-aGFP$_{6M}$-PPP1CA (Figure 2A), FLAG-aGFP$_{6M}$-PPP1CA^{H125Q} (Figure 2A), FLAG-aGFP$_{6M}$-PPP2CA (Figure 2B), or FLAG-aGFP$_{6M}$-PPP2CA^{H118Q} (Figure 2B), a reduction in Cyclin B1 and HMMR levels was observed 3–6 h after STLC washout, similar to that seen in FLAG-empty control cells, suggesting that the expression of FLAG-aGFP$_{6M}$-PPP1CA or FLAG-aGFP$_{6M}$-PPP2CA does not negatively impact the cell cycle-dependent regulation of Cyclin B1 or HMMR. Interestingly, a reduction in the rate of decrease in FAM83D-GFP protein levels following STLC washout was evident in cells expressing FLAG-aGFP$_{6M}$-PPP1CA and FLAG-aGFP$_{6M}$-PPP2CA compared with the corresponding phosphatase-dead mutants or FLAG-empty control cells (Figures 2A and 2B). This suggests that the rate of degradation of mitotic phospho-FAM83D-GFP caused by the proteasome following STLC release[28] is impaired by the AdPhosphatase-mediated dephosphorylation of phospho-FAM83D-GFP.

Finally, to investigate the localization of FAM83D-GFP and CK1α at the mitotic spindle following AdPhosphatase-mediated phospho-FAM83D-GFP dephosphorylation, U2OS *FAM83D* KO[28] and *FAM83D*$^{GFP/GFP}$ cells expressing FLAG-empty, FLAG-aGFP$_{6M}$-PPP1CA, FLAG-aGFP$_{6M}$-PPP1CA^{H125Q}, FLAG-aGFP$_{6M}$-PPP2CA, or FLAG-aGFP$_{6M}$-PPP2CA^{H118Q} were synchronized using STLC, fixed, and analyzed by anti-CK1α and anti-FLAG immunostaining as well as GFP fluorescence microscopy (Figure 2C), and relative CK1α spindle fluorescence intensity was quantified (Figure 2D). As expected, a significant reduction in CK1α levels at the mitotic spindle was observed in *FAM83D* KO cells compared with *FAM83D*$^{GFP/GFP}$ cells (Figures 2C and 2D). Overlapping FAM83D-GFP, CK1α and FLAG localization signals were observed at the mitotic spindle in *FAM83D*$^{GFP/GFP}$ cells expressing FLAG-aGFP$_{6M}$-PPP1CA, FLAG-aGFP$_{6M}$-PPP1CA^{H125Q}, FLAG-aGFP$_{6M}$-PPP2CA, or FLAG-aGFP$_{6M}$-PPP2CA^{H118Q} (Figures 2C and 2D). These observations suggest that the AdPhosphatase-mediated dephosphorylation of phospho-FAM83D-GFP does not interfere with the mitotic localization of either FAM83D-GFP or CK1α. Interestingly, a significant increase in CK1α levels at the mitotic spindle was observed in cells expressing FLAG-aGFP$_{6M}$-PPP2CA compared with FLAG-empty controls and FLAG-aGFP$_{6M}$-PPP2CA^{H118Q} (Figures 2C and 2D), potentially due to stabilization of FAM83D-GFP upon targeted dephosphorylation.

PPP2CA AdPhosphatase targets phospho-GFP-ULK1 for dephosphorylation

To investigate the versatility and broader applicability of the AdPhosphatase system, we next targeted phospho-ULK1 for targeted dephosphorylation. FLAG-aGFP$_{6M}$-PPP1CA or FLAG-aGFP$_{6M}$-PPP2CA was therefore expressed by retroviral transduction in *ULK1*$^{GFP/GFP}$ ARPE-19 cells[33] to direct PPP1CA or PPP2CA to GFP-ULK1 for targeted dephosphorylation of phospho-GFP-ULK1 and to assess the impact on downstream autophagy signaling (Figure 3A). First, to determine the interaction between GFP-ULK1 and FLAG-aGFP$_{6M}$-PPP1CA or FLAG-aGFP$_{6M}$-PPP2CA, extracts from ARPE-19 WT control or *ULK1*$^{GFP/GFP}$ cells expressing FLAG-empty, FLAG-aGFP$_{6M}$-PPP1CA, or FLAG-aGFP$_{6M}$-PPP2CA were subjected to anti-FLAG IP (Figure 3B). GFP-ULK1 co-precipitated with IPs only from *ULK1*$^{GFP/GFP}$ cell extracts expressing FLAG-aGFP$_{6M}$-PPP1CA or FLAG-aGFP$_{6M}$-PPP2CA, but not from WT cells or

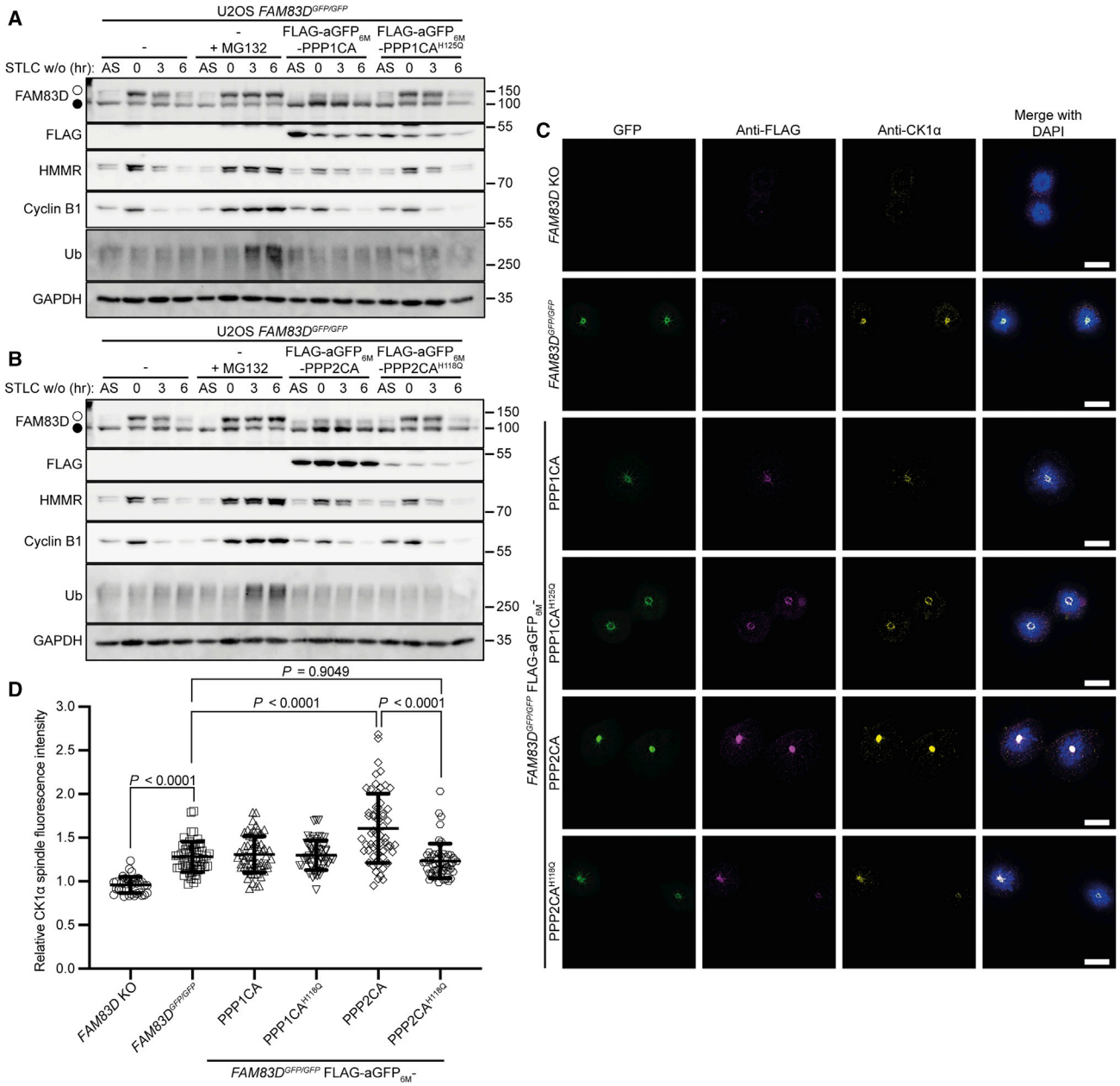

Figure 2. AdPhosphatase-mediated dephosphorylation of mitotic phospho-FAM83D prevents degradation of FAM83D

(A and B) U2OS *FAM83D*$^{GFP/GFP}$ FLAG-empty, FLAG-aGFP$_{6M}$-PPP1CA, FLAG-aGFP$_{6M}$-PPP1CA^{H125Q}, FLAG-aGFP$_{6M}$-PPP2CA, or FLAG-aGFP$_{6M}$-PPP2CA^{H118Q} expressing cells were synchronized in mitosis using the Eg5 inhibitor S-trityl-L-cysteine (STLC) (5 μM) for 16 h. Following incubation, mitotic (M) cells were isolated through shake-off and lysed at indicated time points following STLC washout (w/o) and release into medium ± the proteasomal inhibitor MG132 (20 μM), where stated. Asynchronous (AS) cells were included as a control. Extracts were resolved by SDS-PAGE and transferred onto PVDF membranes, which were subjected to immunoblotting with indicated antibodies. Closed circle denotes non-mitotic FAM83D-GFP, open circle denotes mitotic FAM83D-GFP.

(C) U2OS *FAM83D* knockout (KO) (n = 38) and *FAM83D*$^{GFP/GFP}$ FLAG-empty (n = 55), FLAG-aGFP$_{6M}$-PPP1CA (n = 61), FLAG-aGFP$_{6M}$-PPP1CA^{H125Q} (n = 56), FLAG-aGFP$_{6M}$-PPP2CA (n = 59), or FLAG-aGFP$_{6M}$-PPP2CA^{H118Q} (n = 56) expressing cells were synchronized in mitosis using STLC and subjected to GFP fluorescence and anti-FLAG and anti-CK1α immunofluorescence microscopy. DNA is stained with DAPI. Scale bars, 10 μm.

(D) Quantification of CK1α spindle localization for the cells described in (C) ± SD. Statistical analysis was carried out on the indicated number of cells by one-way ANOVA using Tukey's post-test, n = 2 independent experiments.

ULK1$^{GFP/GFP}$ cells expressing FLAG-empty control, confirming that FLAG-aGFP$_{6M}$-PPP1CA or FLAG-aGFP$_{6M}$-PPP2CA can interact only with GFP-ULK1, but not with untagged ULK1. In addition, both ATG13 and FIP200 co-precipitated in extracts from *ULK1*$^{GFP/GFP}$ cells expressing FLAG-aGFP$_{6M}$-PPP1CA or FLAG-aGFP$_{6M}$-PPP2CA, suggesting that the expression of

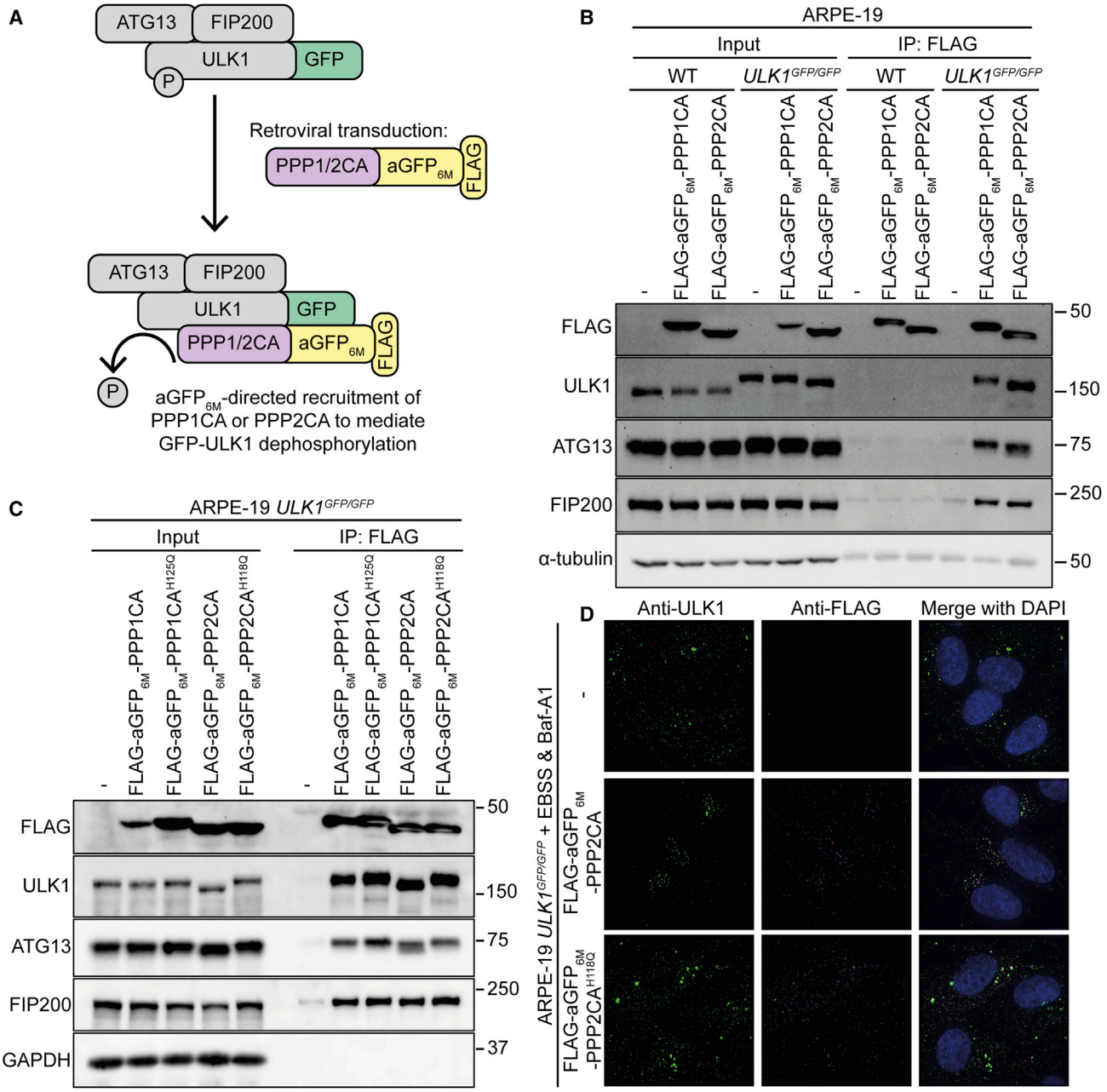

Figure 3. PPP2CA AdPhosphatase targets phospho-GFP-ULK1 for dephosphorylation

(A) Schematic representation of anti-GFP nanobody ($aGFP_{6M}$)-directed recruitment of either PPP1CA or PPP2CA to GFP-tagged ULK1 to mediate phospho-GFP-ULK1 dephosphorylation.

(B) ARPE-19 wild-type (WT) and *ULK1*$^{GFP/GFP}$ knockin cells expressing FLAG-empty, FLAG-$aGFP_{6M}$-PPP1CA, or FLAG-$aGFP_{6M}$-PPP2CA were lysed and subjected to immunoprecipitation (IP) with anti-FLAG M2 resin. * = heavy chain of IgG.

(C) ARPE-19 *ULK1*$^{GFP/GFP}$ cells expressing FLAG-empty, FLAG-$aGFP_{6M}$-PPP1CA, FLAG-$aGFP_{6M}$-PPP1CA^{H125Q}, FLAG-$aGFP_{6M}$-PPP2CA, or FLAG-$aGFP_{6M}$-PPP2CA^{H118Q} were lysed and subjected to IP using anti-FLAG M2 resin.

For (B and C), extracts and IPs were resolved by SDS-PAGE and transferred on to PVDF membranes, which were subjected to immunoblotting with indicated antibodies.

(D) ARPE-19 *ULK1*$^{GFP/GFP}$ cells expressing FLAG-empty, FLAG-$aGFP_{6M}$-PPP2CA, or FLAG-$aGFP_{6M}$-PPP2CA^{H118Q} were starved of amino acids with EBSS and treated with the lysosomal inhibitor Bafilomycin A1 (Baf-A1, 50 nM) for 2 h and subjected to anti-ULK1 and anti-FLAG immunofluorescence microscopy. DNA is stained with DAPI. Scale bars, 10 μm.

either FLAG-aGFP$_{6M}$-PPP1CA or FLAG-aGFP$_{6M}$-PPP2CA does not interfere with the formation of the GFP-ULK1-ATG13-FIP200 complex. Interestingly, a striking downward electrophoretic mobility shift of GFP-ULK1 and ATG13 was observed in extracts from *ULK1*$^{GFP/GFP}$ cells expressing FLAG-aGFP$_{6M}$-PPP2CA, but not FLAG-aGFP$_{6M}$-PPP1CA, suggesting potential dephosphorylation of both phospho-GFP-ULK1 and phospho-ATG13 by FLAG-aGFP$_{6M}$-PPP2CA.

To confirm if the observed GFP-ULK1 dephosphorylation was reliant on the catalytic activity of the AdPhosphatase system, constructs containing the catalytically dead PPP1CA (FLAG-aGFP$_{6M}$-PPP1CA^{H125Q}) or PPP2CA (FLAG-aGFP$_{6M}$-PPP2CA^{H118Q}) mutants were expressed by retroviral transduction in ARPE-19 *ULK1*$^{GFP/GFP}$ cells (Figure 3C). Following anti-FLAG IP, GFP-ULK1, ATG13, and FIP200 co-precipitated with IPs from *ULK1*$^{GFP/GFP}$ cells expressing FLAG-aGFP$_{6M}$-PPP1CA, FLAG-aGFP$_{6M}$-PPP1CA^{H125Q}, FLAG-aGFP$_{6M}$-PPP2CA, or FLAG-aGFP$_{6M}$-PPP2CA^{H118Q}, indicating that the catalytically dead AdPhosphatase constructs also interact with GFP-ULK1 and do not interfere with the formation of the ULK1 complex. Under these conditions, neither FLAG-aGFP$_{6M}$-PPP1CA nor FLAG-aGFP$_{6M}$-PPP1CA^{H125Q} caused any detectable GFP-ULK1 or ATG13 mobility shift. Furthermore, the downward GFP-ULK1 and ATG13 electrophoretic mobility shift evident in FLAG-aGFP$_{6M}$-PPP2CA expressing cells was not observed in FLAG-aGFP$_{6M}$-PPP2CA^{H118Q} expressing cells, suggesting that this potential dephosphorylation-induced mobility shift is reliant on PPP2CA catalytic activity of the AdPhosphatase. ARPE-19 *ULK1*$^{GFP/GFP}$ cells expressing FLAG-empty control or FLAG-aGFP$_{6M}$-PPP2CA were also treated with the protein phosphatase inhibitors Cal A or Okadaic acid (OA)[37,38,42,43] (Figure S2B). In FLAG-empty or FLAG-aGFP$_{6M}$-PPP2CA expressing cells, an increase in Akt S473 phosphorylation levels was observed upon Cal A or OA treatment compared with DMSO-treated controls, suggesting effective protein phosphatase inhibition. No changes in GFP-ULK1 or ATG13 mobility shift, or abundance, were apparent in FLAG-empty cells upon Cal A or OA treatment, compared with DMSO-treated controls. In contrast, in cells expressing FLAG-aGFP$_{6M}$-PPP2CA, the downward GFP-ULK1 and ATG13 electrophoretic mobility shift observed in DMSO-treated cells was restored back to the levels seen in FLAG-empty cells upon treatment with Cal A, suggesting that the AdPhosphatase-mediated dephosphorylation of most of the phospho-sites on GFP-ULK1 and phospho-ATG13 is dependent on the phosphatase activity of FLAG-aGFP$_{6M}$-PPP2CA. In comparison, the restoration of phospho-ULK1 and phospho-ATG13 mobility shifts was less robust with OA treatment, suggesting potential incomplete inhibition of FLAG-aGFP$_{6M}$-PPP2CA by OA or possible off-target effects of OA on kinases that phosphorylate ULK1 or ATG13 responsible for mobility shifts.

Next, we sought to investigate the localization of GFP-ULK1 following AdPhosphatase-mediated GFP-ULK1 dephosphorylation. Upon starvation, ULK1 forms punctate structures that co-localize with omegasomes, thereby supporting autophagosome biogenesis.[44,45] ARPE-19 *ULK1*$^{GFP/GFP}$ cells expressing FLAG-empty, FLAG-aGFP$_{6M}$-PPP2CA, or FLAG-aGFP$_{6M}$-PPP2CA^{H118Q} were starved of amino acids with Earle's balanced salt solution (EBSS) and treated with the lysosomal inhibitor Bafilomycin-A1 (Baf-A1, 50 nM) to prevent autophagosome clearance[46–48] for 2 h, fixed, and analyzed using anti-ULK1 and anti-FLAG immunostaining (Figure 3D). Under these conditions, ULK1 punctate structures were observed in ARPE-19 *ULK1*$^{GFP/GFP}$ cells expressing FLAG-empty, FLAG-aGFP$_{6M}$-PPP2CA, or FLAG-aGFP$_{6M}$-PPP2CA^{H118Q}. In addition, FLAG punctate structures, some of which overlapped with ULK1 puncta, were also observed in *ULK1*$^{GFP/GFP}$ cells expressing FLAG-aGFP$_{6M}$-PPP2CA or FLAG-aGFP$_{6M}$-PPP2CA^{H118Q}.

AdPhosphatase-mediated dephosphorylation of phospho-GFP-ULK1 inhibits starvation-induced autophagy

Under nutrient-rich conditions, human ULK1 is phosphorylated at multiple sites, including S758 (equivalent to mouse S757) by mTORC1, to inhibit autophagy.[49] During periods of starvation, mTORC1 is inactivated and the inhibitory phospho-sites on ULK1 are removed, resulting in increased ULK1 kinase activity.[49] This leads to downstream autophagy signaling, including phosphorylation of ATG13 at S318 by activated ULK1,[50] expansion of the autophagosome, marked by lipidated microtubule-associated protein 1A/1B-light chain 3 (LC3-II), which engulfs cargo and then fuses with the lysosome for cargo degradation.[32] To investigate the effects of aGFP$_{6M}$-PPP2CA-directed dephosphorylation of GFP-ULK1 on downstream starvation-induced autophagy signaling, ARPE-19 *ULK1*$^{GFP/GFP}$ cells expressing FLAG-empty, FLAG-aGFP$_{6M}$-PPP2CA, or FLAG-aGFP$_{6M}$-PPP2CA^{H118Q} were starved of amino acids for 2 h with EBSS (Figures 4A, 4B, and S3). During this period, cells were also treated with Baf-A1 to inhibit lysosomal degradation and monitor autophagic flux.[46–48] As expected, in EBSS-starved *ULK1*$^{GFP/GFP}$ cells expressing FLAG-empty control, a reduction in GFP-ULK1 phosphorylation at S758 with a concomitant increase in ATG13 phosphorylation at S318 was observed compared with amino acid-rich controls, indicating ULK1 activation. However, in FLAG-aGFP$_{6M}$-PPP2CA expressing cells under amino acid-rich conditions, a substantial reduction in basal phosphorylation of ULK1 at S758 was observed compared with FLAG-empty control cells, but a concomitant increase in phosphorylation of ATG13 at S318 was not observed. Furthermore, the EBSS-induced phosphorylation of ATG13 at S318 evident in FLAG-empty control cells was absent in cells expressing FLAG-aGFP$_{6M}$-PPP2CA. Moreover, inhibition of both basal and starvation-induced autophagy signaling was observed in cells expressing FLAG-aGFP$_{6M}$-PPP2CA, as indicated by the large reduction in LC3-II flux, compared with FLAG-empty control cells. These results suggest that one or more phospho-residues on ULK1, other than S758, that are critical for ULK1 activation are also targeted for dephosphorylation by the AdPhosphatase, resulting in the inhibition of ULK1. Indeed, in FLAG-aGFP$_{6M}$-PPP2CA-expressing cells, regardless of amino acid starvation, a complete loss of ULK1 phosphorylation at S555 and S638 was evident compared with FLAG-empty control or FLAG-aGFP$_{6M}$-PPP2CA^{H118Q}-expressing cells (Figure S4). In EBSS-stimulated cells expressing the FLAG-aGFP$_{6M}$-PPP2CA^{H118Q} catalytically dead mutant, robust ATG13 phosphorylation at S318 was observed, comparable to that observed in cells expressing FLAG-empty control (Figures 4A, 4B, and S3). Furthermore, in cells expressing FLAG-aGFP$_{6M}$-PPP2CA^{H118Q}, both basal and starvation-induced LC3-II flux were comparable to cells expressing FLAG-empty control. These data serve to

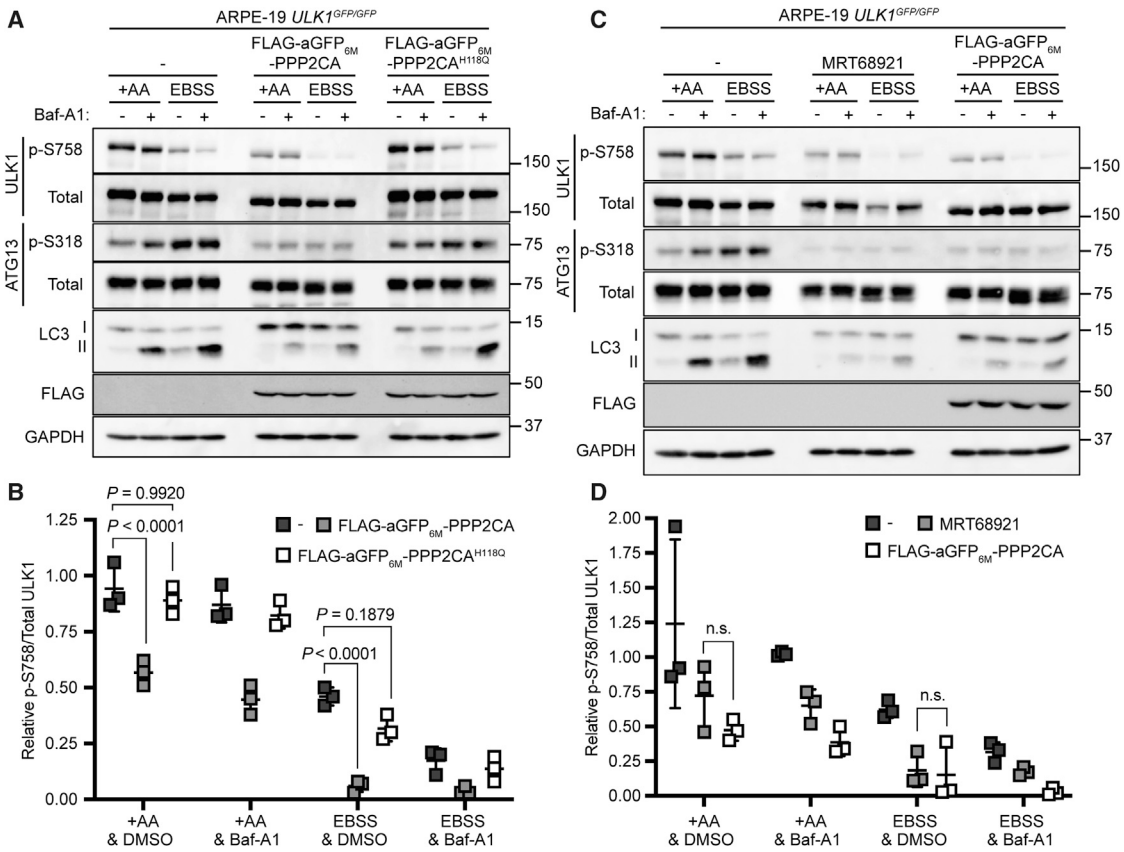

Figure 4. AdPhosphatase-mediated dephosphorylation of phospho-GFP-ULK1 inhibits starvation-induced autophagy

(A) ARPE-19 *ULK1*$^{GFP/GFP}$ cells expressing FLAG-empty, FLAG-aGFP$_{6M}$-PPP2CA, or FLAG-aGFP$_{6M}$-PPP2CA^{H118Q} were starved of amino acids with EBSS and treated with Baf-A1 (50 nM) for 2 h

(B) Quantification of p-S758 ULK1 normalized to total ULK1 protein levels from (A) ± SD of n = 3 independent experiments.

(C) ARPE-19 *ULK1*$^{GFP/GFP}$ cells expressing FLAG-empty or FLAG-aGFP$_{6M}$-PPP2CA were pre-treated with the ULK1 inhibitor MRT68921 (2 μM, 2 h), where indicated, and amino acid starved with EBSS and treated with Baf-A1 (50 nM) for 2 h.

(D) Quantification of p-S758 ULK1 normalized to total ULK1 protein levels from (C) ± SD of n = 3 independent experiments. For (A) and (C), extracts were resolved by SDS-PAGE and transferred onto PVDF membranes, which were subjected to immunoblotting with indicated antibodies. +AA = amino acid-rich conditions, n.s. = not significant. Statistical analyses were carried out by one-way ANOVA using Tukey's post-test.

demonstrate that the reduction in ATG13 S318 phosphorylation and basal and starvation-induced LC3-II flux observed in cells expressing FLAG-aGFP$_{6M}$-PPP2CA is dependent on FLAG-aGFP$_{6M}$-PPP2CA catalytic activity.

Next, we sought to compare the efficacy of autophagy inhibition by AdPhosphatase-directed dephosphorylation of GFP-ULK1 to that of GFP-ULK1 inhibition using the small molecule ULK1 inhibitor MRT68921.[45,51] ARPE-19 *ULK1*$^{GFP/GFP}$ cells expressing FLAG-empty control were pre-treated with or without MRT68921 (2 μM, 2 h) and, along with cells expressing FLAG-aGFP$_{6M}$-PPP2CA that were not treated with MRT68921, were starved of amino acids with EBSS and treated with or without Baf-A1 (50 nM) for 2 h (Figures 4C, 4D, and S5). Under starvation conditions, a comparable reduction in ULK1 phosphorylation at S758 was observed between MRT68921-treated cells and those expressing FLAG-aGFP$_{6M}$-PPP2CA. Furthermore, the reduction in ATG13 phosphorylation at S318 with EBSS relative to amino acid-rich controls was comparable between MRT68921-treated FLAG-empty control cells and DMSO-treated cells expressing FLAG-aGFP$_{6M}$-PPP2CA. In addition, under starvation conditions, LC3-II levels were comparable between MRT68921-treated FLAG-empty control cells and DMSO-treated cells expressing FLAG-aGFP$_{6M}$-PPP2CA. These data suggest that the attenuation of starvation-induced autophagy observed following AdPhosphatase-mediated GFP-ULK1 dephosphorylation reflects that observed when cells were treated with a small molecule inhibitor of ULK1.

FLAG-aGFP$_{6M}$-PPP2CA expression mediates the recruitment of PP2A regulatory subunits

PP2A catalytic C subunits typically only exist in a complex with a scaffold/structural A subunit (PP2A A) and regulatory B subunits, of which there are 26.[52–54] The nature of the PP2A holoenzyme complex determines substrate specificity, subcellular localization, and catalytic activity.[52–55] To determine whether FLAG-aGFP$_{6M}$-PPP2CA exists by itself, or recruits additional scaffold and regulatory subunits, to mediate POI dephosphorylation, STLC-synchronized U2OS *FAM83D*$^{GFP/GFP}$ cells (Figure S1A) or EBSS-starved ARPE-19 *ULK1*$^{GFP/GFP}$ cells (Figure S1B) expressing FLAG-aGFP$_{6M}$-PPP2CA extracts were subjected to anti-FLAG IP. The resultant anti-FLAG IPs were

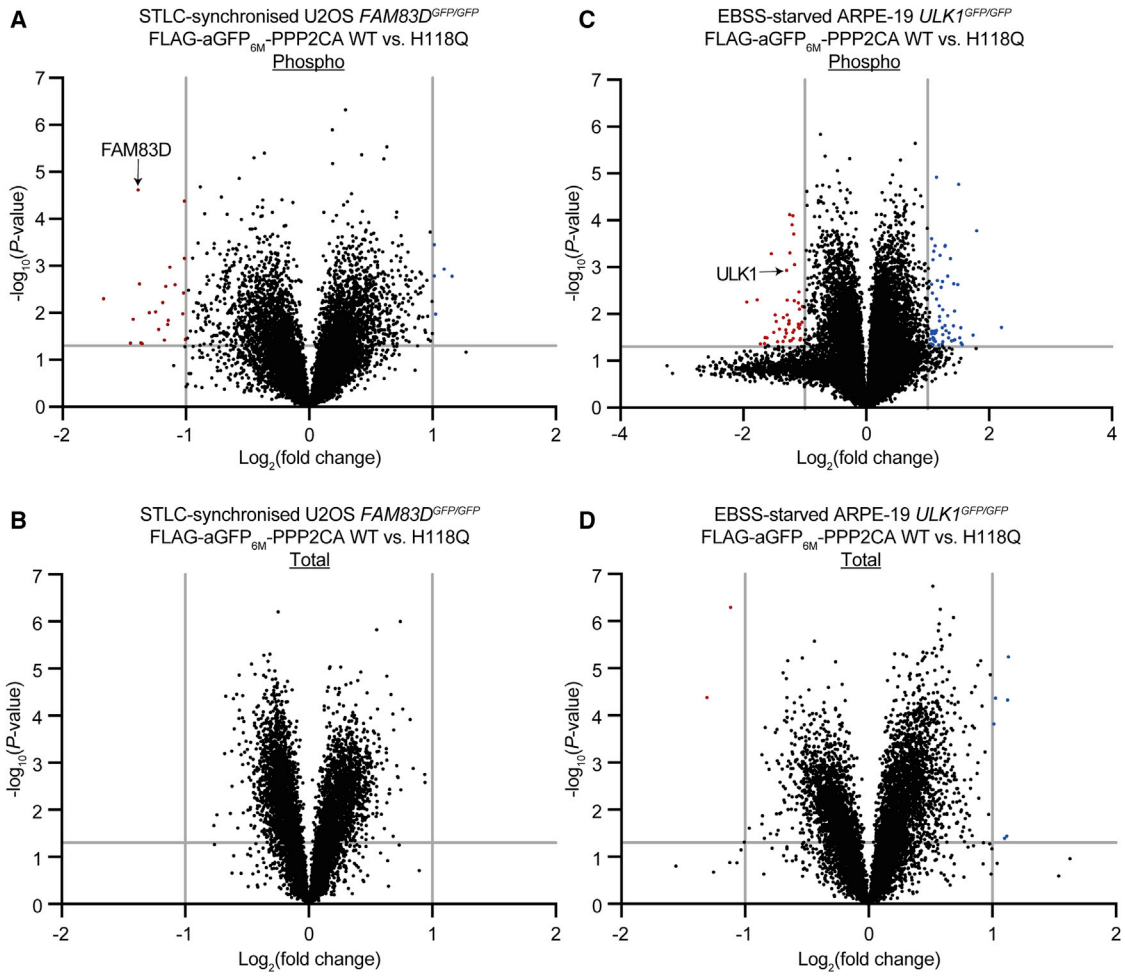

Figure 5. TMT-labeled quantitative global phospho-proteomic analysis of FLAG-aGFP$_{6M}$-PPP2CA AdPhosphatase-mediated FAM83D-GFP and GFP-ULK1 dephosphorylation

Volcano plot following global (A) phospho- (11,821 unique phospho-peptides detected) and (B) total- (7,201 proteins detected) proteomic analysis of STLC-synchronized U2OS *FAM83D*$^{GFP/GFP}$ cells expressing FLAG-aGFP$_{6M}$-PPP2CA compared with those expressing FLAG-aGFP$_{6M}$-PPP2CA^{H118Q}. Volcano plot following global (C) phospho- (22,574 unique phospho-peptides detected) and (D) total- (8,153 proteins detected) proteomic analysis of EBSS-starved ARPE-19 *ULK1*$^{GFP/GFP}$ cells expressing FLAG-aGFP$_{6M}$-PPP2CA compared with those expressing FLAG-aGFP$_{6M}$-PPP2CA^{H118Q}. Gray horizontal threshold indicates significance level of p = 0.05. Gray vertical threshold indicates 2-fold change. The top left quadrant indicates phospho-peptides/peptides that are hypo-phosphorylated/downregulated in cells expressing FLAG-aGFP$_{6M}$-PPP2CA over those expressing FLAG-aGFP$_{6M}$-PPP2CA^{H118Q}, colored red, whereas the top right quadrant indicates phospho-peptides/peptides that are hyper-phosphorylated/upregulated in cells expressing FLAG-aGFP$_{6M}$-PPP2CA over those expressing FLAG-aGFP$_{6M}$-PPP2CA^{H118Q}, colored blue. Phospho-peptide detected corresponding to FAM83D is labeled in (A), and ULK1 is labeled in (C).

resolved by SDS-PAGE, subjected to in-gel trypsin digestion, and the resulting peptides were analyzed by LC-MS/MS (Figure S1C). FLAG-aGFP$_{6M}$-PPP2CA interactors identified exclusively from mitotic U2OS *FAM83D*$^{GFP/GFP}$ cells included FAM83D, CK1α, and HMMR (Figure S1C), which were validated by western blot (Figure S1A), whereas those identified exclusively from EBSS-starved ARPE-19 *ULK1*$^{GFP/GFP}$ cells included ULK1, ATG13, and FIP200 (Figure S1C), which were also validated by western blot (Figure S1B). Interestingly, FLAG-aGFP$_{6M}$-PPP2CA interactors identified that were common to both mitotic U2OS *FAM83D*$^{GFP/GFP}$ and EBSS-starved ARPE-19 *ULK1*$^{GFP/GFP}$ cells included PPP2CA (bait), the PP2A 65 kDa regulatory subunit A alpha (PPP2R1A) and beta (PPP2R1B) isoforms, the PP2A 55 kDa regulatory subunit B alpha isoform (PPP2R2A), and the PP2A 56 kDa regulatory subunit delta (PPP2R5D) and epsilon (PPP2R5E) isoforms (Figure S1C). These data suggest that, as reported previously for PPP2CA,[52–55] the FLAG-aGFP$_{6M}$-PPP2CA AdPhosphatase does not appear to exist by itself, but rather recruits additional regulatory subunits to mediate targeted dephosphorylation of phospho-FAM83D-GFP and phospho-GFP-ULK1.

Global phospho-proteomics demonstrates remarkable specificity of the FLAG-aGFP$_{6M}$-PPP2CA AdPhosphatase system

To determine the specificity of the FLAG-aGFP$_{6M}$-PPP2CA AdPhosphatase-mediated dephosphorylation of phospho-FAM83D-GFP in mitosis or phospho-GFP-ULK1 following amino acid starvation, an unbiased global phospho-proteomic approach was used (Figure 5). U2OS *FAM83D*$^{GFP/GFP}$ cells expressing

Table 1. Phospho-peptides corresponding to FAM83D identified following global phospho-proteomic analysis of AdPhosphatase-mediated FAM83D-GFP dephosphorylation

Protein	UniProt ID	Phospho-peptide	Fold change	p value
FAM83D	Q9H4H8	SSSSVSSQGSVASSTGSPASIR (S493)	0.38	<0.001
		GTQSTEGSPVSK (S462)	0.50	0.001
		KPHDCESSTVSEEDYFSSHRDELQSR (S369)	0.63	0.032

Values of phospho-peptides corresponding to FAM83D identified from global analysis of STLC-synchronized U2OS *FAM83D*$^{GFP/GFP}$ cells expressing FLAG-aGFP$_{6M}$-PPP2CA compared with FLAG-aGFP$_{6M}$-PPP2CA^{H118Q}. The corresponding FAM83D phospho-peptide detected is indicated, as is the fold change and p value.

FLAG-aGFP$_{6M}$-PPP2CA or FLAG-aGFP$_{6M}$-PPP2CA^{H118Q} were synchronized in mitosis with STLC and subjected to quantitative phospho- and total-proteomic analyses (Figures 5A and 5B). Following total protein analysis of STLC-synchronized U2OS *FAM83D*$^{GFP/GFP}$ cells expressing FLAG-aGFP$_{6M}$-PPP2CA compared with those expressing FLAG-aGFP$_{6M}$-PPP2CA^{H118Q} (Figure 5B), a total of 7,201 proteins were identified and of those, no proteins were observed to significantly change in abundance more than 2-fold between the two conditions. This suggests that the expression of FLAG-aGFP$_{6M}$-PPP2CA, compared with FLAG-aGFP$_{6M}$-PPP2CA^{H118Q}, in U2OS *FAM83D*$^{GFP/GFP}$ cells does not cause any substantial changes to total protein levels. Following phospho-peptide enrichment and analysis of STLC-synchronized U2OS *FAM83D*$^{GFP/GFP}$ cells expressing FLAG-aGFP$_{6M}$-PPP2CA compared with those expressing FLAG-aGFP$_{6M}$-PPP2CA^{H118Q} (Figure 5A, Tables 1 and S1), 11,821 unique phospho-peptides were identified. Of these, levels of phospho-peptides corresponding to 21 proteins were significantly downregulated by more than 2-fold, and six were significantly upregulated by more than 2-fold, in U2OS *FAM83D*$^{GFP/GFP}$ cells expressing FLAG-aGFP$_{6M}$-PPP2CA compared with those expressing FLAG-aGFP$_{6M}$-PPP2CA^{H118Q}. Of the significantly downregulated phospho-peptides detected in FLAG-aGFP$_{6M}$-PPP2CA-expressing cells, two FAM83D phospho-peptides were detected (pS493 and pS462). FAM83D pS369 was also found to be significantly downregulated, but not by more than 2-fold. Further work is needed to determine whether phosphorylation of FAM83D at pS369, pS493, and/or pS462 mediates FAM83D proteasomal degradation following mitotic exit. Of the other phospho-peptides identified, some corresponding to mitosis-regulating proteins, including INCENP (inner centromere protein),[56–61] were found to be downregulated.

Next, ARPE-19 *ULK1*$^{GFP/GFP}$ cells expressing FLAG-aGFP$_{6M}$-PPP2CA or FLAG-aGFP$_{6M}$-PPP2CA^{H118Q} were starved of amino acids with EBSS for 2 h to remove mTORC1-mediated ULK1 inhibition and subjected to quantitative phospho- and total-proteomic analyses (Figures 5C and 5D). Following total protein analysis of EBSS-starved ARPE-19 *ULK1*$^{GFP/GFP}$ cells expressing FLAG-aGFP$_{6M}$-PPP2CA compared with those expressing FLAG-aGFP$_{6M}$-PPP2CA^{H118Q} (Figure 5D and Table S2), a total of 8,153 proteins were identified, and of these, levels of three proteins were significantly downregulated by more than 2-fold between the two conditions, whereas levels of three other proteins were significantly upregulated. Whether the observed changes in the abundance of these six proteins is a direct consequence of GFP-ULK1 dephosphorylation needs to be further investigated. Following phospho-peptide enrichment and analysis of EBSS-starved ARPE-19 *ULK1*$^{GFP/GFP}$ cells expressing FLAG-aGFP$_{6M}$-PPP2CA compared with those expressing FLAG-aGFP$_{6M}$-PPP2CA^{H118Q} (Figure 5C, Tables 2 and S3), 22,574 unique phospho-peptides were identified. Of these, levels of phospho-peptides corresponding to 43 proteins were significantly downregulated by more than 2-fold, and 63 were significantly upregulated by more than 2-fold, in ARPE-19 *ULK1*$^{GFP/GFP}$ cells expressing FLAG-aGFP$_{6M}$-PPP2CA compared with those expressing FLAG-aGFP$_{6M}$-PPP2CA^{H118Q}. Of the significantly downregulated phospho-peptides detected in FLAG-aGFP$_{6M}$-PPP2CA expressing cells, three ULK1 phospho-residues were detected, including S539, S544, and S694. The levels of ULK1 phospho-residues T468, S623, S638, and S758 were also found to be significantly downregulated, but not by more than 2-fold. Further work is needed to determine whether phosphorylation of ULK1 at these residues impacts its role in starvation-induced autophagy. Of the other phospho-peptides identified, those corresponding to autophagy-regulating proteins, including Beclin-1, a previously reported ULK1 substrate,[62,63] AP-3 complex subunit beta-1 (AP3B1),[64] and La-related protein 1 (LARP1),[65] were found to be downregulated. Whether the alteration observed in the phospho-peptides corresponding to these or other proteins is a direct consequence of GFP-ULK1 dephosphorylation and inactivation or rather due to being in proximity of FLAG-aGFP$_{6M}$-PPP2CA needs to be further investigated. To test this, we evaluated the *in vitro* kinase activity of GFP-ULK1 associated with anti-FLAG IPs from ARPE-19 *ULK1*$^{GFP/GFP}$ cells expressing FLAG-aGFP$_{6M}$, FLAG-aGFP$_{6M}$-PPP2CA, or FLAG-aGFP$_{6M}$-PPP2CA^{H118Q} against recombinant ATG13 and found no substantial differences in the levels of phosphorylation of recombinant ATG13, potentially suggesting that the proximity of the phosphatase to ATG13 rather than the kinase activity of ULK1 might have resulted in the AdPhosphatase-mediated dephosphorylation of ATG13 in cells (Figure S6).

DISCUSSION

Through the conjugation of a high-affinity polypeptide binder of GFP to a catalytic subunit of a phosphatase (AdPhosphatase), we demonstrate here that phosphatase catalytic activity can be redirected to endogenously GFP-tagged proteins FAM83D and ULK1 to mediate targeted phospho-POI dephosphorylation with exquisite selectivity. By directing an AdPhosphatase construct consisting of aGFP$_{6M}$ conjugated to PPP1CA or PPP2CA to FAM83D-GFP in *FAM83D*$^{GFP/GFP}$ cells, dephosphorylation of phospho-FAM83D-GFP was promoted in mitosis to delay phosphorylation-triggered FAM83D-GFP degradation. Using the

Table 2. Phospho-peptides corresponding to ULK1 identified following global phospho-proteomic analysis of AdPhosphatase-mediated GFP-ULK1 dephosphorylation

Protein	UniProt ID	Phospho-peptide	Fold change	p value
ULK1	O75385	SFSTSR (S694)	0.41	0.001
		SPRPGSSAPEHSPR (S539, S544)	0.48	0.033
		SGSTSPLGFAR (T468)	0.71	0.004
		NPLPPILGSPTK (S623)	0.72	<0.001
		TPSSQNLLALLAR (S638)	0.74	0.011
		AGGTSSPSPVVFTVGSPPSGSTPPQGPR (S758)	0.79	0.001

Values of phospho-peptides corresponding to ULK1 identified from global analysis of EBSS-starved ARPE-19 *ULK1*$^{GFP/GFP}$ cells expressing FLAG-aGFP$_{6M}$-PPP2CA compared with FLAG-aGFP$_{6M}$-PPP2CA^{H118Q}. The corresponding ULK1 phospho-peptide detected is indicated, as is the fold change and p value.

AdPhosphatase system, the role of the mitotic CK1α-mediated phosphorylation of FAM83D[28] in its proteolysis was established, highlighting the applicability of the AdPhosphatase system in understanding the function of phospho-modifications on POIs. The PPP2CA AdPhosphatase-mediated dephosphorylation of phospho-FAM83D-GFP in mitotic *FAM83D*$^{GFP/GFP}$ cells was remarkably specific, with only a small list of other phospho-peptides shown to be significantly downregulated in an unbiased global phospho-proteomic screen.

Similarly, an AdPhosphatase construct consisting of aGFP$_{6M}$ conjugated to PPP2CA mediated the targeted dephosphorylation of phospho-GFP-ULK1 when expressed in *ULK1*$^{GFP/GFP}$ cells. AdPhosphatase-mediated GFP-ULK1 dephosphorylation attenuated starvation-induced autophagy to the same extent as chemical inhibition of ULK1. ULK1 undergoes phosphorylation at multiple residues that orchestrate either an activating or inhibitory role on its activity and subsequently its role in autophagy initiation.[32] The PPP2CA AdPhosphatase system resulted in a profound dephosphorylation of phospho-GFP-ULK1 and resulted in the inhibition of starvation-induced autophagy, suggesting that this system targeted the dephosphorylation of dominant ULK1 phospho-residues that potentiate ULK1 activity. Following global phospho-proteomic analysis, three ULK1 phospho-residues, S539, S544, and S694, were found to be significantly downregulated more than 2-fold in EBSS-starved cells expressing FLAG-aGFP$_{6M}$-PPP2CA compared with FLAG-aGFP$_{6M}$-PPP2CA^{H118Q}. Further efforts are required to determine whether phosphorylation of ULK1 at S539, S544, or S694 is necessary for initiating starvation-induced autophagy. In addition, the FLAG-aGFP$_{6M}$-PPP2CA AdPhosphatase system could be further used to determine whether the phosphorylation of ULK1 is involved in the regulation of additional selective forms of autophagy, such as mitophagy, ER-phagy/reticulophagy, pexophagy, ferritinophagy, nucleophagy, lysophagy, lipophagy, glycophagy, aggrephagy, and xenophagy.[66] Also of interest was the observation that the ULK1-mediated phosphorylation of ATG13 at S318 following amino acid starvation was attenuated by the FLAG-aGFP$_{6M}$-PPP2CA AdPhosphatase system.

Interestingly, the AdPhosphatase system consisting of aGFP conjugated to PPP1CA was unable to dephosphorylate ULK1, although it acted to dephosphorylate FAM83D-GFP, suggesting the possibility that PPP1CA may not have access to the same phospho-residues on ULK1 that PPP2CA has. Further investigations are needed to ascertain the range of dephosphorylation activity of the different phosphatases when used with the AdPhosphatase system. The use of apo-phosphatases, such as carboxy-terminal domain RNA polymerase II polypeptide A small phosphatases (CTDSP) 1–3,[67–70] with the AdPhosphatase system could potentially improve the range of target protein dephosphorylation due to removal of the scaffold proteins required for phosphatases that are part of holoenzyme complexes.

As the AdPhosphatase system demonstrates proof-of-concept for efficient targeted dephosphorylation, the end goal for translating targeted dephosphorylation as a potential therapeutic approach would be to develop small molecule phosphorylation-targeting chimeras (PhosTACs) that directly bind the endogenous, untagged POI and recruit an endogenous phosphatase and its activity. Recently, there have been some reports of small molecule and peptide-based phosphatase recruiting chimeras for targeted dephosphorylation.[71–75] Heterobifunctional small molecules recruiting Halo-PP1 linked to selective inhibitors of Akt and EGFR were reported to induce dephosphorylation of Akt and EGFR, respectively, albeit with relatively low efficacy.[71] A tag-based PhosTAC involving a dTAG-/Halo-recruiting heterobifunctional small molecule was also designed recently for chemical proof-of-concept to recruit overexpressed FKBP12^{F36V}-tagged PP2A regulatory subunit to an overexpressed Halo-tagged POI to mediate POI dephosphorylation.[73] To understand whether this dTAG-/Halo-recruiting PhosTAC approach affects endogenous protein function, FKBP12^{F36V} and Halo would need to be knocked-in on to the respective phosphatase subunit and POI using, for example, CRISPR-Cas9 genome editing technology, as long as the tags are tolerated by the respective proteins. A heterobifunctional peptide-based recruiter molecule to facilitate PP2A-Bα and Tau protein proximity to elicit targeted dephosphorylation of Tau, was reported to lead to degradation of Tau.[72] The constitutive AdPhosphatase system described here can be exploited not only to explore the biological role of specific phospho-GFP-POIs, where GFP-tagging is tolerated, but also to inform the suitability of a chosen phosphatase in mediating the targeted dephosphorylation of the substrate of interest, prior to investing in the resource- and time-intensive development of POI-specific dephosphorylation-inducing heterobifunctional small molecules.

Limitations of the study

There are a few limitations of the current AdPhosphatase approach. The AdPhosphatase is introduced in cells via retroviral

transduction and hence the target cell genome is modified randomly. The constitutive expression of the AdPhosphatase means that the interaction between the $aGFP_{6M}$-AdPhosphatase and the GFP-POI and hence the target protein dephosphorylation are also constitutive. In order to use the $aGFP_{6M}$-based AdPhosphatases against a desired intracellular POI, there is a requirement to introduce a GFP tag on the POI by genome editing methodologies, which can be time-consuming and need testing to ensure the GFP-tagging is tolerated.

SIGNIFICANCE

Protein phosphorylation is a fundamental driver of all cell signaling processes and is therefore tightly regulated. Hyperphosphorylation of proteins is a known hallmark of many diseases, including cancer and neurodegenerative diseases. In this study, we describe a new approach termed the AdPhosphatase system, which efficiently and selectively targeted endogenously GFP-tagged FAM83D and ULK1 for dephosphorylation. This AdPhosphatase system is versatile and adaptable, where, in principle, promiscuous phosphatase activity can be redirected toward any intracellular phosphorylated GFP-tagged POI that tolerates a GFP-fusion. If selective nanobodies against endogenous POIs exist, the AdPhosphatase can be adapted to assess targeted dephosphorylation of unmodified POIs. Nonetheless, whether the target protein is dephosphorylated needs to be evaluated on a case-by-case basis. Achieving targeted dephosphorylation of phospho-proteins by small molecule PhosTACs could hold promise as a therapeutic approach, although currently no allosteric ligands against endogenous phosphatases exist. The AdPhosphatase system can inform whether dephosphorylating a target POI by a specific phosphatase alters its function resulting in a desired phenotype so that ligand development for potential PhosTACs can be prioritized.

STAR★METHODS

Detailed methods are provided in the online version of this paper and include the following:

- KEY RESOURCES TABLE
- RESOURCE AVAILABILITY
  - Lead contact
  - Materials availability
  - Data and code availability
- EXPERIMENTAL MODEL AND SUBJECT DETAILS
  - Cell lines
- METHOD DETAILS
  - Plasmids
  - Generation of cell lines using CRISPR/Cas9
  - Retroviral generation of stable cell lines
  - Treatment of cells with compounds
  - Cell lysis and immunoprecipitation
  - SDS-PAGE and Western blotting
  - *In vitro* ULK1 kinase assay
  - Immunofluorescence microscopy
  - Mass spectrometry
- QUANTIFICATION AND STATISTICAL ANALYSIS

SUPPLEMENTAL INFORMATION

Supplemental information can be found online at https://doi.org/10.1016/j.chembiol.2023.01.003.

ACKNOWLEDGMENTS

This study was funded by the UK Medical Research Council (MRC), awarded to G.P.S. (MC_UU_00018/6). G.P.S. is also supported by the pharmaceutical companies supporting the Division of Signal Transduction Therapy (Boehringer-Ingelheim, GlaxoSmithKline, Merck-Serono). We thank members of the G.P.S. Lab for their highly appreciated experimental advice and discussions during the course of these experiments. We thank E. Allen, J. Stark, and A. Muir for assistance with tissue culture; the staff at the DNA Sequencing services (University of Dundee); and the cloning and antibody production teams within the MRC PPU Reagents & Services (University of Dundee) coordinated by J. Hastie. We thank the staff at the Dundee Imaging Facility (University of Dundee) for their invaluable advice throughout this project.

AUTHOR CONTRIBUTIONS

L.M.S. and L.J.F. performed experiments, collected and analyzed data, and contributed to the writing of the manuscript. G.S. assisted with quantitative global total and phospho-proteomics experiments and data analysis. A.B. assisted during the optimization of the AdPhosphatase technology and contributed to the writing of the manuscript. J.Z. performed experiments and collected and analyzed data during the revision of the manuscript. D.R.S. assisted during the optimization of the AdPhosphatase technology. N.W., J.C., and M.W. generated constructs used in this study. J.V., R.G., and R.S. assisted with interactome-based proteomics experiments and data analysis. G.P.S. conceived the project, analyzed data, and contributed to the writing of the manuscript.

DECLARATION OF INTERESTS

The authors declare no competing interests.

INCLUSION AND DIVERSITY

The authors support inclusive, diverse, and equitable conduct of research.

Received: January 13, 2022
Revised: November 7, 2022
Accepted: January 10, 2023
Published: January 30, 2023

REFERENCES

1. Cohen, P. (2002). The origins of protein phosphorylation. Nat. Cell Biol. *4*, E127–E130. https://doi.org/10.1038/ncb0502-e127.
2. Ardito, F., Giuliani, M., Perrone, D., Troiano, G., and Lo Muzio, L. (2017). The crucial role of protein phosphorylation in cell signaling and its use as targeted therapy (Review). Int. J. Mol. Med. *40*, 271–280. https://doi.org/10.3892/ijmm.2017.3036.
3. Ingebritsen, T.S., and Cohen, P. (1983). The protein phosphatases involved in cellular regulation. 1. Classification and substrate specificities. Eur. J. Biochem. *132*, 255–261. https://doi.org/10.1111/j.1432-1033.1983.tb07357.x.
4. Johnson, L.N., and Lewis, R.J. (2001). Structural basis for control by phosphorylation. Chem. Rev. *101*, 2209–2242. https://doi.org/10.1021/cr000225s.
5. Cohen, P. (2001). The role of protein phosphorylation in human health and disease. The Sir Hans Krebs Medal Lecture. Eur. J. Biochem. *268*, 5001–5010. https://doi.org/10.1046/j.0014-2956.2001.02473.x.
6. Cohen, P., Cross, D., and Jänne, P.A. (2021). Kinase drug discovery 20 years after imatinib: progress and future directions. Nat. Rev. Drug Discov. *20*, 551–569. https://doi.org/10.1038/s41573-021-00195-4.

7. Mullard, A. (2018). Phosphatases start shedding their stigma of undruggability. Nat. Rev. Drug Discov. *17*, 847–849. https://doi.org/10.1038/nrd.2018.201.

8. Köhn, M. (2020). Turn and face the strange: a new view on phosphatases. ACS Cent. Sci. *6*, 467–477. https://doi.org/10.1021/acscentsci.9b00909.

9. Fabian, M.A., Biggs, W.H., 3rd, Treiber, D.K., Atteridge, C.E., Azimioara, M.D., Benedetti, M.G., Carter, T.A., Ciceri, P., Edeen, P.T., Floyd, M., et al. (2005). A small molecule-kinase interaction map for clinical kinase inhibitors. Nat. Biotechnol. *23*, 329–336. https://doi.org/10.1038/nbt1068.

10. Fedorov, O., Marsden, B., Pogacic, V., Rellos, P., Müller, S., Bullock, A.N., Schwaller, J., Sundström, M., and Knapp, S. (2007). A systematic interaction map of validated kinase inhibitors with Ser/Thr kinases. Proc. Natl. Acad. Sci. USA *104*, 20523–20528. https://doi.org/10.1073/pnas.0708800104.

11. Karaman, M.W., Herrgard, S., Treiber, D.K., Gallant, P., Atteridge, C.E., Campbell, B.T., Chan, K.W., Ciceri, P., Davis, M.I., Edeen, P.T., et al. (2008). A quantitative analysis of kinase inhibitor selectivity. Nat. Biotechnol. *26*, 127–132. https://doi.org/10.1038/nbt1358.

12. Elkins, J.M., Fedele, V., Szklarz, M., Abdul Azeez, K.R., Salah, E., Mikolajczyk, J., Romanov, S., Sepetov, N., Huang, X.P., Roth, B.L., et al. (2016). Comprehensive characterization of the published kinase inhibitor set. Nat. Biotechnol. *34*, 95–103. https://doi.org/10.1038/nbt.3374.

13. Tsutsumi, R., Ran, H., and Neel, B.G. (2018). Off-target inhibition by active site-targeting SHP2 inhibitors. FEBS Open Bio *8*, 1405–1411. https://doi.org/10.1002/2211-5463.12493.

14. Ferguson, F.M., and Gray, N.S. (2018). Kinase inhibitors: the road ahead. Nat. Rev. Drug Discov. *17*, 353–377. https://doi.org/10.1038/nrd.2018.21.

15. Smyth, L.A., and Collins, I. (2009). Measuring and interpreting the selectivity of protein kinase inhibitors. J. Chem. Biol. *2*, 131–151. https://doi.org/10.1007/s12154-009-0023-9.

16. Munoz, L. (2017). Non-kinase targets of protein kinase inhibitors. Nat. Rev. Drug Discov. *16*, 424–440. https://doi.org/10.1038/nrd.2016.266.

17. Lanning, B.R., Whitby, L.R., Dix, M.M., Douhan, J., Gilbert, A.M., Hett, E.C., Johnson, T.O., Joslyn, C., Kath, J.C., Niessen, S., et al. (2014). A road map to evaluate the proteome-wide selectivity of covalent kinase inhibitors. Nat. Chem. Biol. *10*, 760–767. https://doi.org/10.1038/nchembio.1582.

18. Mandell, D.J., Chorny, I., Groban, E.S., Wong, S.E., Levine, E., Rapp, C.S., and Jacobson, M.P. (2007). Strengths of hydrogen bonds involving phosphorylated amino acid side chains. J. Am. Chem. Soc. *129*, 820–827. https://doi.org/10.1021/ja063019w.

19. Roberts-Galbraith, R.H., Ohi, M.D., Ballif, B.A., Chen, J.S., McLeod, I., McDonald, W.H., Gygi, S.P., Yates, J.R., 3rd, and Gould, K.L. (2010). Dephosphorylation of F-BAR protein Cdc15 modulates its conformation and stimulates its scaffolding activity at the cell division site. Mol. Cell *39*, 86–99. https://doi.org/10.1016/j.molcel.2010.06.012.

20. Beránek, V., Reinkemeier, C.D., Zhang, M.S., Liang, A.D., Kym, G., and Chin, J.W. (2018). Genetically encoded protein phosphorylation in mammalian cells. Cell Chem. Biol. *25*, 1067–1074.e5. https://doi.org/10.1016/j.chembiol.2018.05.013.

21. Brautigan, D.L., and Shenolikar, S. (2018). Protein serine/threonine phosphatases: keys to unlocking regulators and substrates. Annu. Rev. Biochem. *87*, 921–964. https://doi.org/10.1146/annurev-biochem-062917-012332.

22. Olsen, J.V., Blagoev, B., Gnad, F., Macek, B., Kumar, C., Mortensen, P., and Mann, M. (2006). Global, in vivo, and site-specific phosphorylation dynamics in signaling networks. Cell *127*, 635–648. https://doi.org/10.1016/j.cell.2006.09.026.

23. Hoermann, B., Kokot, T., Helm, D., Heinzlmeir, S., Chojnacki, J.E., Schubert, T., Ludwig, C., Berteotti, A., Kurzawa, N., Kuster, B., et al. (2020). Dissecting the sequence determinants for dephosphorylation by the catalytic subunits of phosphatases PP1 and PP2A. Nat. Commun. *11*, 3583. https://doi.org/10.1038/s41467-020-17334-x.

24. Ogris, E., Mudrak, I., Mak, E., Gibson, D., and Pallas, D.C. (1999). Catalytically inactive protein phosphatase 2A can bind to polyomavirus middle tumor antigen and support complex formation with pp60(c-src). J. Virol. *73*, 7390–7398. https://doi.org/10.1128/JVI.73.9.7390-7398.1999.

25. Casamayor, A., and Ariño, J. (2020). Controlling Ser/Thr protein phosphatase PP1 activity and function through interaction with regulatory subunits. Adv. Protein Chem. Struct. Biol. *122*, 231–288. https://doi.org/10.1016/bs.apcsb.2020.06.004.

26. Davey, N.E., Van Roey, K., Weatheritt, R.J., Toedt, G., Uyar, B., Altenberg, B., Budd, A., Diella, F., Dinkel, H., and Gibson, T.J. (2012). Attributes of short linear motifs. Mol. Biosyst. *8*, 268–281. https://doi.org/10.1039/c1mb05231d.

27. Wu, J., Liu, J., Thompson, I., Oliver, C.J., Shenolikar, S., and Brautigan, D.L. (1998). A conserved domain for glycogen binding in protein phosphatase-1 targeting subunits. FEBS Lett. *439*, 185–191. https://doi.org/10.1016/s0014-5793(98)01371-4.

28. Fulcher, L.J., He, Z., Mei, L., Macartney, T.J., Wood, N.T., Prescott, A.R., Whigham, A.J., Varghese, J., Gourlay, R., Ball, G., et al. (2019). FAM83D directs protein kinase CK1alpha to the mitotic spindle for proper spindle positioning. EMBO Rep. *20*, e47495. https://doi.org/10.15252/embr.201847495.

29. Ganley, I.G., Lam, D.H., Wang, J., Ding, X., Chen, S., and Jiang, X. (2009). ULK1.ATG13.FIP200 complex mediates mTOR signaling and is essential for autophagy. J. Biol. Chem. *284*, 12297–12305. https://doi.org/10.1074/jbc.M900573200.

30. Jung, C.H., Jun, C.B., Ro, S.H., Kim, Y.M., Otto, N.M., Cao, J., Kundu, M., and Kim, D.H. (2009). ULK-Atg13-FIP200 complexes mediate mTOR signaling to the autophagy machinery. Mol. Biol. Cell *20*, 1992–2003. https://doi.org/10.1091/mbc.E08-12-1249.

31. Hosokawa, N., Hara, T., Kaizuka, T., Kishi, C., Takamura, A., Miura, Y., Iemura, S.i., Natsume, T., Takehana, K., Yamada, N., et al. (2009). Nutrient-dependent mTORC1 association with the ULK1-Atg13-FIP200 complex required for autophagy. Mol. Biol. Cell *20*, 1981–1991. https://doi.org/10.1091/mbc.E08-12-1248.

32. Zachari, M., and Ganley, I.G. (2017). The mammalian ULK1 complex and autophagy initiation. Essays Biochem. *61*, 585–596. https://doi.org/10.1042/EBC20170021.

33. Simpson, L.M., Macartney, T.J., Nardin, A., Fulcher, L.J., Röth, S., Testa, A., Maniaci, C., Ciulli, A., Ganley, I.G., and Sapkota, G.P. (2020). Inducible degradation of target proteins through a tractable affinity-directed protein missile system. Cell Chem. Biol. *27*, 1164–1180.e5. https://doi.org/10.1016/j.chembiol.2020.06.013.

34. Tang, J.C., Drokhlyansky, E., Etemad, B., Rudolph, S., Guo, B., Wang, S., Ellis, E.G., Li, J.Z., and Cepko, C.L. (2016). Detection and manipulation of live antigen-expressing cells using conditionally stable nanobodies. Elife *5*, e15312. https://doi.org/10.7554/eLife.15312.

35. Hsu, L.C., Huang, X., Seasholtz, S., Potter, D.M., and Gollin, S.M. (2006). Gene amplification and overexpression of protein phosphatase 1alpha in oral squamous cell carcinoma cell lines. Oncogene *25*, 5517–5526. https://doi.org/10.1038/sj.onc.1209563.

36. Gergs, U., Boknik, P., Buchwalow, I., Fabritz, L., Matus, M., Justus, I., Hanske, G., Schmitz, W., and Neumann, J. (2004). Overexpression of the catalytic subunit of protein phosphatase 2A impairs cardiac function. J. Biol. Chem. *279*, 40827–40834. https://doi.org/10.1074/jbc.M405770200.

37. Resjö, S., Oknianska, A., Zolnierowicz, S., Manganiello, V., and Degerman, E. (1999). Phosphorylation and activation of phosphodiesterase type 3B (PDE3B) in adipocytes in response to serine/threonine phosphatase inhibitors: deactivation of PDE3B in vitro by protein phosphatase type 2A. Biochem. J. *341*, 839–845.

38. Ishihara, H., Martin, B.L., Brautigan, D.L., Karaki, H., Ozaki, H., Kato, Y., Fusetani, N., Watabe, S., Hashimoto, K., Uemura, D., et al. (1989). Calyculin A and okadaic acid: inhibitors of protein phosphatase activity.

Biochem. Biophys. Res. Commun. *159*, 871–877. https://doi.org/10.1016/0006-291x(89)92189-x.

39. Egloff, M.P., Cohen, P.T., Reinemer, P., and Barford, D. (1995). Crystal structure of the catalytic subunit of human protein phosphatase 1 and its complex with tungstate. J. Mol. Biol. *254*, 942–959. https://doi.org/10.1006/jmbi.1995.0667.

40. Ogris, E., Du, X., Nelson, K.C., Mak, E.K., Yu, X.X., Lane, W.S., and Pallas, D.C. (1999). A protein phosphatase methylesterase (PME-1) is one of several novel proteins stably associating with two inactive mutants of protein phosphatase 2A. J. Biol. Chem. *274*, 14382–14391. https://doi.org/10.1074/jbc.274.20.14382.

41. Chang, D.C., Xu, N., and Luo, K.Q. (2003). Degradation of cyclin B is required for the onset of anaphase in Mammalian cells. J. Biol. Chem. *278*, 37865–37873. https://doi.org/10.1074/jbc.M306376200.

42. Cohen, P., Klumpp, S., and Schelling, D.L. (1989). An improved procedure for identifying and quantitating protein phosphatases in mammalian tissues. FEBS Lett. *250*, 596–600. https://doi.org/10.1016/0014-5793(89)80803-8.

43. Fernández, J.J., Candenas, M.L., Souto, M.L., Trujillo, M.M., and Norte, M. (2002). Okadaic acid, useful tool for studying cellular processes. Curr. Med. Chem. *9*, 229–262. https://doi.org/10.2174/0929867023371247.

44. Karanasios, E., Stapleton, E., Manifava, M., Kaizuka, T., Mizushima, N., Walker, S.A., and Ktistakis, N.T. (2013). Dynamic association of the ULK1 complex with omegasomes during autophagy induction. J. Cell Sci. *126*, 5224–5238. https://doi.org/10.1242/jcs.132415.

45. Zachari, M., Longo, M., and Ganley, I.G. (2020). Aberrant autophagosome formation occurs upon small molecule inhibition of ULK1 kinase activity. Life Sci. Alliance *3*, e202000815. https://doi.org/10.26508/lsa.202000815.

46. Yoshimori, T., Yamamoto, A., Moriyama, Y., Futai, M., and Tashiro, Y. (1991). Bafilomycin A1, a specific inhibitor of vacuolar-type H(+)-ATPase, inhibits acidification and protein degradation in lysosomes of cultured cells. J. Biol. Chem. *266*, 17707–17712.

47. Mauvezin, C., Nagy, P., Juhász, G., and Neufeld, T.P. (2015). Autophagosome-lysosome fusion is independent of V-ATPase-mediated acidification. Nat. Commun. *6*, 7007. https://doi.org/10.1038/ncomms8007.

48. Klionsky, D.J., Abdelmohsen, K., Abe, A., Abedin, M.J., Abeliovich, H., Acevedo Arozena, A., Adachi, H., Adams, C.M., Adams, P.D., Adeli, K., et al. (2016). Guidelines for the use and interpretation of assays for monitoring autophagy (3rd edition). Autophagy *12*, 1–382. https://doi.org/10.1080/15548627.2015.1100356.

49. Kim, J., Kundu, M., Viollet, B., and Guan, K.L. (2011). AMPK and mTOR regulate autophagy through direct phosphorylation of Ulk1. Nat. Cell Biol. *13*, 132–141. https://doi.org/10.1038/ncb2152.

50. Joo, J.H., Dorsey, F.C., Joshi, A., Hennessy-Walters, K.M., Rose, K.L., McCastlain, K., Zhang, J., Iyengar, R., Jung, C.H., Suen, D.F., et al. (2011). Hsp90-Cdc37 chaperone complex regulates Ulk1- and Atg13-mediated mitophagy. Mol. Cell *43*, 572–585. https://doi.org/10.1016/j.molcel.2011.06.018.

51. Petherick, K.J., Conway, O.J.L., Mpamhanga, C., Osborne, S.A., Kamal, A., Saxty, B., and Ganley, I.G. (2015). Pharmacological inhibition of ULK1 kinase blocks mammalian target of rapamycin (mTOR)-dependent autophagy. J. Biol. Chem. *290*, 11376–11383. https://doi.org/10.1074/jbc.C114.627778.

52. Janssens, V., and Goris, J. (2001). Protein phosphatase 2A: a highly regulated family of serine/threonine phosphatases implicated in cell growth and signalling. Biochem. J. *353*, 417–439. https://doi.org/10.1042/0264-6021:3530417.

53. Mumby, M. (2007). PP2A: unveiling a reluctant tumor suppressor. Cell *130*, 21–24. https://doi.org/10.1016/j.cell.2007.06.034.

54. Seshacharyulu, P., Pandey, P., Datta, K., and Batra, S.K. (2013). Phosphatase: PP2A structural importance, regulation and its aberrant expression in cancer. Cancer Lett. *335*, 9–18. https://doi.org/10.1016/j.canlet.2013.02.036.

55. Lambrecht, C., Haesen, D., Sents, W., Ivanova, E., and Janssens, V. (2013). Structure, regulation, and pharmacological modulation of PP2A phosphatases. Methods Mol. Biol. *1053*, 283–305. https://doi.org/10.1007/978-1-62703-562-0_17.

56. Adams, R.R., Eckley, D.M., Vagnarelli, P., Wheatley, S.P., Gerloff, D.L., Mackay, A.M., Svingen, P.A., Kaufmann, S.H., and Earnshaw, W.C. (2001). Human INCENP colocalizes with the Aurora-B/AIRK2 kinase on chromosomes and is overexpressed in tumour cells. Chromosoma *110*, 65–74. https://doi.org/10.1007/s004120100130.

57. Li, X., Sakashita, G., Matsuzaki, H., Sugimoto, K., Kimura, K., Hanaoka, F., Taniguchi, H., Furukawa, K., and Urano, T. (2004). Direct association with inner centromere protein (INCENP) activates the novel chromosomal passenger protein, Aurora-C. J. Biol. Chem. *279*, 47201–47211. https://doi.org/10.1074/jbc.M403029200.

58. Honda, R., Körner, R., and Nigg, E.A. (2003). Exploring the functional interactions between Aurora B, INCENP, and survivin in mitosis. Mol. Biol. Cell *14*, 3325–3341. https://doi.org/10.1091/mbc.e02-11-0769.

59. Sasai, K., Katayama, H., Hawke, D.H., and Sen, S. (2016). Aurora-C interactions with survivin and INCENP reveal shared and distinct features compared with aurora-B chromosome passenger protein complex. PLoS One *11*, e0157305. https://doi.org/10.1371/journal.pone.0157305.

60. Kang, J., Chaudhary, J., Dong, H., Kim, S., Brautigam, C.A., and Yu, H. (2011). Mitotic centromeric targeting of HP1 and its binding to Sgo1 are dispensable for sister-chromatid cohesion in human cells. Mol. Biol. Cell *22*, 1181–1190. https://doi.org/10.1091/mbc.E11-01-0009.

61. Qi, W., Tang, Z., and Yu, H. (2006). Phosphorylation- and polo-box-dependent binding of Plk1 to Bub1 is required for the kinetochore localization of Plk1. Mol. Biol. Cell *17*, 3705–3716. https://doi.org/10.1091/mbc.e06-03-0240.

62. Russell, R.C., Tian, Y., Yuan, H., Park, H.W., Chang, Y.Y., Kim, J., Kim, H., Neufeld, T.P., Dillin, A., and Guan, K.L. (2013). ULK1 induces autophagy by phosphorylating Beclin-1 and activating VPS34 lipid kinase. Nat. Cell Biol. *15*, 741–750. https://doi.org/10.1038/ncb2757.

63. Qian, X., Li, X., Cai, Q., Zhang, C., Yu, Q., Jiang, Y., Lee, J.-H., Hawke, D., Wang, Y., Xia, Y., et al. (2017). Phosphoglycerate kinase 1 phosphorylates Beclin1 to induce autophagy. Mol. Cell *65*, 917–931.e6. https://doi.org/10.1016/j.molcel.2017.01.027.

64. Kannangara, A.R., Poole, D.M., McEwan, C.M., Youngs, J.C., Weerasekara, V.K., Thornock, A.M., Lazaro, M.T., Balasooriya, E.R., Oh, L.M., Soderblom, E.J., et al. (2021). BioID reveals an ATG9A interaction with ATG13-ATG101 in the degradation of p62/SQSTM1-ubiquitin clusters. EMBO Rep. *22*, e51136. https://doi.org/10.15252/embr.202051136.

65. McKnight, N.C., Jefferies, H.B.J., Alemu, E.A., Saunders, R.E., Howell, M., Johansen, T., and Tooze, S.A. (2012). Genome-wide siRNA screen reveals amino acid starvation-induced autophagy requires SCOC and WAC. EMBO J. *31*, 1931–1946. https://doi.org/10.1038/emboj.2012.36.

66. Gatica, D., Lahiri, V., and Klionsky, D.J. (2018). Cargo recognition and degradation by selective autophagy. Nat. Cell Biol. *20*, 233–242. https://doi.org/10.1038/s41556-018-0037-z.

67. Yeo, M., Lin, P.S., Dahmus, M.E., and Gill, G.N. (2003). A novel RNA polymerase II C-terminal domain phosphatase that preferentially dephosphorylates serine 5. J. Biol. Chem. *278*, 26078–26085. https://doi.org/10.1074/jbc.M301791200.

68. Yeo, M., Lee, S.K., Lee, B., Ruiz, E.C., Pfaff, S.L., and Gill, G.N. (2005). Small CTD phosphatases function in silencing neuronal gene expression. Science *307*, 596–600. https://doi.org/10.1126/science.1100801.

69. Kamenski, T., Heilmeier, S., Meinhart, A., and Cramer, P. (2004). Structure and mechanism of RNA polymerase II CTD phosphatases. Mol. Cell *15*, 399–407. https://doi.org/10.1016/j.molcel.2004.06.035.

70. Zhang, Y., Kim, Y., Genoud, N., Gao, J., Kelly, J.W., Pfaff, S.L., Gill, G.N., Dixon, J.E., and Noel, J.P. (2006). Determinants for dephosphorylation of the RNA polymerase II C-terminal domain by Scp1. Mol. Cell *24*, 759–770. https://doi.org/10.1016/j.molcel.2006.10.027.

71. Yamazoe, S., Tom, J., Fu, Y., Wu, W., Zeng, L., Sun, C., Liu, Q., Lin, J., Lin, K., Fairbrother, W.J., and Staben, S.T. (2020). Heterobifunctional molecules induce dephosphorylation of kinases-A proof of concept study. J. Med. Chem. *63*, 2807–2813. https://doi.org/10.1021/acs.jmedchem.9b01167.

72. Zheng, J., Tian, N., Liu, F., Zhang, Y., Su, J., Gao, Y., Deng, M., Wei, L., Ye, J., Li, H., and Wang, J.Z. (2021). A novel dephosphorylation targeting chimera selectively promoting tau removal in tauopathies. Signal Transduct. Target. Ther. *6*, 269. https://doi.org/10.1038/s41392-021-00669-2.

73. Chen, P.-H., Hu, Z., An, E., Okeke, I., Zheng, S., Luo, X., Gong, A., Jaime-Figueroa, S., and Crews, C.M. (2021). Modulation of phosphoprotein activity by phosphorylation targeting chimeras (PhosTACs). ACS Chem. Biol. *16*, 2808–2815. https://doi.org/10.1021/acschembio.1c00693.

74. Conway, S.J. (2020). Bifunctional molecules beyond PROTACs. J. Med. Chem. *63*, 2802–2806. https://doi.org/10.1021/acs.jmedchem.0c00293.

75. Zhang, Q., Wu, X., Zhang, H., Wu, Q., Fu, M., Hua, L., Zhu, X., Guo, Y., Zhang, L., You, Q., and Wang, L. (2022). Protein phosphatase 5-recruiting chimeras for accelerating apoptosis-signal-regulated kinase 1 dephosphorylation with antiproliferative activity. J. Am. Chem. Soc. https://doi.org/10.1021/jacs.2c10759.

76. Schneider, C.A., Rasband, W.S., and Eliceiri, K.W. (2012). NIH Image to ImageJ: 25 years of image analysis. Nat. Methods *9*, 671–675. https://doi.org/10.1038/nmeth.2089.

77. Allan, C., Burel, J.M., Moore, J., Blackburn, C., Linkert, M., Loynton, S., Macdonald, D., Moore, W.J., Neves, C., Patterson, A., et al. (2012). OMERO: flexible, model-driven data management for experimental biology. Nat. Methods *9*, 245–253. https://doi.org/10.1038/nmeth.1896.

78. Cong, L., Ran, F.A., Cox, D., Lin, S., Barretto, R., Habib, N., Hsu, P.D., Wu, X., Jiang, W., Marraffini, L.A., and Zhang, F. (2013). Multiplex genome engineering using CRISPR/Cas systems. Science *339*, 819–823. https://doi.org/10.1126/science.1231143.

STAR★METHODS

KEY RESOURCES TABLE

REAGENT or RESOURCE	SOURCE	IDENTIFIER
Antibodies		
Rabbit polyclonal anti-Akt	Cell Signaling Technology	Cat# 9272S, RRID:AB_329827
Mouse monoclonal anti-Akt p-S473	Cell Signaling Technology	Cat# 12694, RRID:AB_2797994
Rabbit polyclonal anti-ATG13	Sigma-Aldrich	Cat# SAB4200100, RRID:AB_10602787
Rabbit polyclonal anti-ATG13 p-S318	Novus	Cat# NBP2-19127
Rabbit polyclonal anti-CK1 alpha	Bethyl	Cat# A301-991A, RRID:AB_1576501
Sheep monoclonal anti-CK1 alpha	MRC PPU Reagents & Services	Cat# SA527
Rabbit polyclonal anti-Cyclin B1	Cell Signaling Technology	Cat# 4138, RRID:AB_2072132
Sheep monoclonal anti-FAM83D	MRC PPU Reagents & Services	Cat# SA102
Rabbit polyclonal anti-FIP200	Proteintech	Cat# 17250-1-AP, RRID:AB_10666428
Mouse monoclonal anti-FLAG, HRP-conjugated	Sigma-Aldrich	Cat# A8592, RRID:AB_439702
Mouse monoclonal anti-FLAG	Sigma-Aldrich	Cat# F1804, RRID:AB_262044
Rabbit monoclonal anti-DYKDDDDK Tag (FLAG)	Cell Signaling Technology	Cat# 14793, RRID:AB_2572291
Rabbit monoclonal anti-GAPDH	Cell Signaling Technology	Cat# 2118, RRID:AB_561053
Sheep monoclonal anti-GFP	MRC PPU Reagents & Services	Cat# S268B
Rabbit monoclonal anti-HMMR	Abcam	Cat# ab124729, RRID:AB_10975797
Sheep monoclonal anti-LC3	MRC PPU Reagents & Services	Cat# S400D
Mouse monoclonal anti-mono- and poly-ubiquitinylated conjugates	Enzo Life Sciences	Cat# BML-PW8810, RRID:AB_2051891
Sheep monoclonal anti-PPP2CA	MRC PPU Reagents & Services	Cat# S274B
Rat monoclonal anti-alpha-tubulin	Thermo Fisher Scientific	Cat# MA1-80189, RRID:AB_2210200
Rabbit monoclonal anti-ULK1	Cell Signaling Technology	Cat# 8054, RRID:AB_11178668
Rabbit monoclonal anti-ULK1 p-S555	Cell Signaling Technology	Cat# 5869, RRID:AB_10707365
Rabbit monoclonal anti-ULK1 p-S638	Cell Signaling Technology	Cat# 14205, RRID:AB_2798424
Rabbit monoclonal anti-ULK1 p-S757	Cell Signaling Technology	Cat# 6888, RRID:AB_10829226
Goat anti-mouse IgG (H+L), HRP-linked	Thermo Fisher Scientific	Cat# 31430, RRID:AB_228307
Goat anti-rabbit IgG, HRP-linked	Cell Signaling Technology	Cat# 7074S, RRID:AB_2099233
Goat anti-rat IgG (H+L), HRP-linked	Thermo Fisher Scientific	Cat# 62-9520, RRID:AB_87993
Rabbit anti-sheep IgG HRP-conjugated	Thermo Fisher Scientific	Cat# 31480, RRID:AB_228457
Donkey anti-rabbit IgG Alexa Fluor™ 488	Thermo Fisher Scientific	Cat# A21206, RRID:AB_2535792
Goat anti-mouse IgG Alexa Fluor™ 594	Thermo Fisher Scientific	Cat# A11005, RRID:AB_2534073
Goat anti-rabbit IgG Alexa Fluor™ 594	Thermo Fisher Scientific	Cat# A11012, RRID:AB_2534079
Donkey anti-sheep IgG Alexa Fluor™ 647	Thermo Fisher Scientific	Cat# A21448, RRID:AB_2535865
Chemicals, peptides, and recombinant proteins		
MG132, proteasome inhibitor	Abcam	Cat# ab141003
Calyculin A (Cal A)	Cell Signaling Technology	Cat# 9902
Okadaic acid (OA)	Cell Signaling Technology	Cat# 5934
Bafilomycin A1 (Baf A1)	Enzo Life Sciences	Cat# BML-CM110
MRT68921	MRC PPU Reagents & Services	N/A
S-trityl-L-cysteine (STLC)	Sigma-Aldrich	Cat# 164739
GST-ATG13	MRC PPU Reagents & Services	Cat# DU30086
PEI MAX – Transfection Grade Linear PEI Hydrochloride MW 40,000	Polysciences	Cat# 24765
Polybrene (Hexadimethrine bromide)	Sigma-Aldrich	Cat# 107689
GFP-Trap-Agarose	Chromotek	Cat# GTA-20, RRID:AB_2631357

(*Continued on next page*)

Continued		
REAGENT or RESOURCE	SOURCE	IDENTIFIER
Anti-FLAG M2 Affinity Gel	Sigma-Aldrich	Cat# A2220, RRID:AB_10063035
Immobilon Western Chemiluminescent HRP Substrate	Merck	Cat# WBKLS0500
ProLong™ Gold Antifade Mountant with DAPI	Life Technologies	Cat# P36935
Pierce Trypsin Protease, MS Grade	ThermoFisher	Cat# 90058
Critical commercial assays		
TMT10plex Isobaric Label Reagent Set	ThermoFisher	Cat# 90110
Deposited data		
The proteomics data generated during this study	This paper	PRIDE Archive Accession Number: PXD039200
Data obtained in this study	This paper	https://data.mendeley.com/datasets/sz5kk7p48w/draft?a=65411f4e-79bb-4803-9b1e-311144cca870
Experimental models: Cell lines		
Human: ARPE-19	ATCC	Cat# CRL-2302
Human: ARPE-19 *ULK1*$^{GFP/GFP}$	Simpson et al.[33]	N/A
Human: HEK293-FT	Invitrogen	Cat#R70007
Human: U2OS	ATCC	HTB-96
Human: U2OS *FAM83D*$^{GFP/GFP}$	Fulcher et al.[28]	N/A
Human: U2OS *FAM83D* KO	Fulcher et al.[28]	N/A
Recombinant DNA		
pCMV5-gag-pol	Cell Biolabs	Cat# RV-111
pCMV5-VSV-G	Cell Biolabs	Cat# RV-110
pBabeD-puromycin FLAG-aGFP$_{6M}$	MRC PPU Reagents & Services	DU57701
pBabeD-puromycin FLAG-aGFP$_{6M}$-PPP1CA	MRC PPU Reagents & Services	DU62917
pBabeD-puromycin FLAG-aGFP$_{6M}$-PPP1CA^{H125Q}	MRC PPU Reagents & Services	DU62964
pBabeD-puromycin FLAG-aGFP$_{6M}$-PPP2CA	MRC PPU Reagents & Services	DU62902
pBabeD-puromycin FLAG-aGFP$_{6M}$-PPP2CA^{H118Q}	MRC PPU Reagents & Services	DU62960
Software and algorithms		
ImageJ	Schneider et al.[76]	https://imagej.net
GraphPad Prism v9.4.0	GraphPad	https://www.graphpad.com/scientific-software/prism/
OMERO 5.4.10	Allan et al.[77]	https://openmicroscopy.org/
SoftWoRx	GE Healthcare	N/A

RESOURCE AVAILABILITY

Lead contact

Further information and requests for resources and reagents should be directed to and will be fulfilled by the lead contact, Gopal Sapkota (g.sapkota@dundee.ac.uk).

Materials availability

All constructs used in this study are available to request from the MRC PPU Reagents & Services webpage (http://mrcppureagents.dundee.ac.uk) and the unique identifier (DU) numbers provide direct links to the cloning strategies and sequence details. All constructs were sequence-verified by the DNA Sequencing Service, University of Dundee (http://www.dnaseq.co.uk).

Data and code availability

- Unprocessed Western blot and immunofluorescence data and proteomics data have been deposited at Mendeley Data and PRIDE, respectively, and are publicly available as of the date of publication. Accession numbers are listed in the key resources table.
- This paper does not report original code.
- Any additional information required to reanalyze the data reported in this paper is available from the lead contact upon request.

EXPERIMENTAL MODEL AND SUBJECT DETAILS

Cell lines

All procedures were carried out under aseptic conditions meeting biological safety requirements. ARPE-19 cells (ATCC, Cat# CRL-2302) are human retinal pigment epithelial cells derived from a 19-year-old male. HEK293-FT cells (Invitrogen, Cat# R70007) are a clonal isolate of HEK293 cells transformed with the SV40 large T antigen. U2OS cells (ATCC, Cat# HTB-96) are human epithelial bone osteosarcoma cells derived from a 15-year-old Caucasian female. For growth, HEK293-FT and U2OS cells were maintained in DMEM (Life Technologies) containing 10% (v/v) foetal bovine serum (FBS, Thermo Fisher Scientific), 2 mM L-glutamine (Lonza), 100 U/ml penicillin (Lonza) and 0.1 mg/mL streptomycin (Lonza). ARPE-19 cells were maintained in a 1:1 mix of DMEM and Ham's F-12 nutrient mix (Life Technologies) containing 15% (v/v) FBS, 2 mM L-glutamine, 100 U/ml penicillin and 0.1 mg/mL streptomycin. Cells were grown at 37°C with 5% CO_2 in a water-saturated incubator. For passaging, cells were incubated with trypsin/EDTA at 37°C to detach cells.

METHOD DETAILS

Plasmids

For production of retroviral vectors, the following were cloned into pBABED-puromycin plasmids: FLAG-aGFP$_{6M}$ (DU57701), FLAG-aGFP$_{6M}$-PPP1CA (DU62917), FLAG-aGFP$_{6M}$-PPP1CA^{H125Q} (DU62964), FLAG-aGFP$_{6M}$-PPP2CA (DU62902), FLAG-aGFP$_{6M}$-PPP2CA^{H118Q} (DU62960). All constructs were sequence-verified by the DNA Sequencing Service, University of Dundee (http://www.dnaseq.co.uk). These constructs are available to request from the MRC PPU Reagents and Services webpage (http://mrcppureagents.dundee.ac.uk) and the unique identifier (DU) numbers provide direct links to the cloning strategies and sequence details.

Generation of cell lines using CRISPR/Cas9

The CRISPR/Cas9 genome editing system[78] was used to generate U2OS *FAM83D* homozygous C-terminal GFP knockin (KI) (*FAM83D*$^{GFP/GFP}$) cells,[28] *FAM83D* knock-out (*FAM83D* KO) cells,[28] and ARPE-19 *ULK1* homozygous N-terminal GFP KI (*ULK1*$^{GFP/GFP}$) cells.[33] For *FAM83D* KO cells, U2OS cells were transfected with vectors encoding a pair of guide RNAs (pBABED-Puro-sgRNA1 and pX335-CAS9-D10A-sgRNA2) targeting around the first exon of FAM83D (1 μg each) along with 1 mg/mL PEI. For *FAM83D*$^{GFP/GFP}$ cells, U2OS cells were transfected with vectors encoding a pair of guide RNAs (pBABED-Puro-sgRNA1 and pX335-CAS9-D10A-sgRNA2) targeting around the stop codon of FAM83D, along with the respective donor plasmid carrying the GFP KI insert and flanking homology arms (~500 bases) (3 μg each) and PEI. For *ULK1*$^{GFP/GFP}$ cells, ARPE-19 cells were transfected with vectors encoding a pair of guide RNAs (pBABED-puromycin-sgRNA1 and pX335-CAS9-D10A-sgRNA2) targeting ULK1 exon 1 (1 mg each), along with the respective donor plasmids carrying the GFP KI insert (3 mg) and PEI. 16 hr post-transfection, selection with 2 μg/mL puromycin (Sigma-Aldrich) was carried out and continued for a further 48 hr. The transfection process was repeated one more time. After selection, cells were sorted by flow cytometry and single GFP-positive cell clones were plated on individual wells of two 96-well plates. Viable clones were expanded, and integration of GFP at the target locus was verified by Western blotting and genomic sequencing of the targeted locus.

Retroviral generation of stable cell lines

Retroviral pBABED-puromycin vectors encoding the desired construct (6 μg) were co-transfected with pCMV5-gag-pol (3.2 μg) and pCMV5-VSV-G (2.8 μg) (Cell Biolabs) into a 10 cm diameter dish of ~70% confluent HEK293-FT cells. Briefly, plasmids were added to 1 mL Opti-MEM medium to which 24 μL of 1 mg/mL PEI was added. Following a gentle mix and incubation at room temperature for 20 min, the transfection mix was added dropwise to HEK293-FT cells. 16 hr post-transfection, fresh medium was added to the cells. 24 hr later, the retroviral medium was collected and passed through 0.45 μm sterile syringe filters. Target cells (~60% confluent) were transduced with the optimised titre of the retroviral medium diluted in fresh medium (typically 1:1-1:10) containing 8 μg/ml polybrene (Sigma-Aldrich) for 24 hr. The retroviral medium was then replaced with fresh medium, and 24 hr later, the medium was again replaced with fresh medium containing 2 μg/ml puromycin for selection of cells which had integrated the constructs. A pool of transduced cells were utilised for subsequent experiments following complete death of non-transduced cells placed under selection in parallel.

Treatment of cells with compounds

The following chemicals were added to cell media at indicated concentrations and times: MG132 (Abcam), Calyculin A (CST), Okadaic acid (CST), Bafilomycin-A1 (Enzo Life Sciences), MRT68921 (MRC PPU Reagents and Services). Cells were synchronised in mitosis using the Eg5 inhibitor S-trityl-L-cysteine (STLC, Sigma-Aldrich, 5 μM, 16 hr).[28,33] Following incubation, mitotic cells were lysed after isolation through shake-off or after release into fresh media containing stated compounds for indicated times. For amino acid starvation, cells were washed twice in Earle's balanced salt solution (EBSS, Gibco) and incubated in EBSS for 2 hr.

Cell lysis and immunoprecipitation

Cells were harvested by washing twice with phosphate-buffered saline (PBS) and scraping into ice-cold lysis buffer (50 mM Tris-HCl pH 7.5, 0.27 M sucrose, 150 mM NaCl, 1 mM EGTA, 1 mM EDTA, 1 mM sodium orthovanadate, 10 mM sodium β-glycerophosphate,

50 mM sodium fluoride, 5 mM sodium pyrophosphate and 1% NP-40) supplemented with 1x cOmplete™ protease inhibitor cocktail (Roche). After incubation for 10 min on ice, lysates were clarified by centrifugation at 20,000 xg for 20 min at 4°C. Protein concentration was determined according to the Bradford assay to enable normalisation between samples.

Following determination of protein concentration by Bradford assay, immunoprecipitation (IP) was utilised to isolate a particular protein of interest. For anti-FLAG IPs, anti-FLAG M2 resin (Sigma-Aldrich) was used; for anti-GFP IPs, GFP-TRAP beads (ChromoTek) were used. Before an IP was performed, an input from each lysate was retained to compare and determine IP efficiency. Samples were incubated for 4 hr at 4°C on a rotating wheel. Beads were collected by centrifugation at 1000 xg for 1 min at 4°C and a sample of the supernatant was retained (flow-through). IPs were subsequently washed three times with lysis buffer. Input, IP and flow-through samples were reduced in LDS sample buffer (Invitrogen).

SDS-PAGE and Western blotting

Cell lysates containing equal amounts of protein (10-20 μg) were resolved by SDS-PAGE and transferred to PVDF membrane. Membranes were blocked in 5% (w/v) non-fat milk (Marvel) in TBS-T (50 mM Tris–HCl pH 7.5, 150 mM NaCl, 0.2% Tween-20) and incubated overnight at 4°C in 5% (w/v) BSA/TBS-T or 5% (w/v) milk/TBS-T with the appropriate primary antibodies. Primary antibodies used at indicated dilutions include: anti-Akt (9272S, CST, 1:1,000), anti-Akt p-S473 (12694, CST, 1:1,000), anti-ATG13 (SAB4200100, Sigma-Aldrich, 1:1,000), anti-ATG13 p-S318 (NBP2-19127, Novus, 1:1,000), anti-CK1α (A301-991A, Bethyl, 1:1,000; SA527, MRC PPU Reagents & Services, 1:1,000), anti-Cyclin B1 (4138, CST, 1:1,000), anti-FAM83D (SA102, MRC PPU Reagents & Services, 1:1,000), anti-FIP200 (17250-1-AP, Proteintech, 1:1,000), anti-FLAG (A8592, Sigma-Aldrich, 1:2,500), anti-GAPDH (2118, CST, 1:5,000), anti-GFP (S268B, MRC PPU Reagents & Services, 1:2,000), anti-HMMR (ab124729, Abcam), anti-LC3 (S400D, MRC PPU Reagents & Services, 1:200), anti-mono- and poly-ubiquitinylated conjugates (BML-PW8810, Enzo Life Sciences, 1:2,000), anti-PPP2CA (S274B, MRC PPU Reagents & Services, 1:1,000), anti-α-tubulin (MA1-80189, Thermo Fisher Scientific, 1:5,000), anti-ULK1 (8054, CST, 1:1,000), anti-ULK1 p-S555 (5869, CST, 1:1,000), anti-ULK1 p-S638 (14205, CST, 1:1,000), anti-ULK1 p-S757 (6888, CST, 1:1,000).

Membranes were subsequently washed with TBS-T and incubated with HRP-conjugated secondary antibody for 1 hr at room temperature. HRP-coupled secondary antibodies used at indicated dilutions include: goat anti-rabbit-IgG (7074, CST, 1:2,500), rabbit anti-sheep-IgG (31480, Thermo Fisher Scientific, 1:5,000), goat anti-rat IgG (62-9520, Thermo Fisher Scientific, 1:5,000), goat anti-mouse-IgG (31430, Thermo Fisher Scientific, 1:5,000). After further washing, signal detection was performed using ECL (Merck) and ChemiDoc MP System (Bio-Rad). ImageJ v1.49 (National Institutes of Health) was used to analyse protein bands by densitometry.[76]

In vitro ULK1 kinase assay

ARPE-19 *ULK1*$^{GFP/GFP}$ cells expressing FLAG-aGFP$_{6M}$, FLAG-aGFP$_{6M}$-PPP2CA or FLAG-aGFP$_{6M}$-PPP2CA^{H118Q} were lysed and subjected to IP with anti-FLAG M2 resin to co-IP GFP-ULK1. Following IP, resins were washed twice with lysis buffer and twice with kinase assay buffer (1 mM DTT, 50 mM $NaCl_2$, 50mM Tris-HCl pH 7.5, 1 mM EGTA, 1 mM $MgCl_2$). Resins were then incubated within kinase assay buffer containing 100 mM [γ-^{32}P]ATP (~500 cpm/pmol) and 2 μg of GST-ATG13 (DU30086, MRC PPU Reagents and Services). Reactions were incubated at 30°C for 30 min with shaking, and terminated by adding 2x SDS sample buffer containing 5% (v/v) β-mercaptoethanol and subsequent heating at 95°C for 5 min.

Immunofluorescence microscopy

Cells were seeded onto sterile glass coverslips in 6-well dishes. Coverslips were washed twice with PBS, fixed with 4% (w/v) paraformaldehyde (Thermo Fisher Scientific) for 10 min, washed twice with and incubated for 10 min in DMEM/10 mM HEPES pH 7.4. After one wash in PBS, cell permeabilisation was carried out using 0.2% NP-40 in PBS for 4 min. Samples were blocked by washing twice and incubation for 15 min in blocking buffer (1% (w/v) BSA/PBS). Coverslips were incubated for 1 hr at 37°C with primary antibodies in blocking buffer and washed three times in blocking buffer. Mouse anti-FLAG monoclonal (F1804, Sigma-Aldrich), rabbit anti-DYKDDDDK Tag (FLAG) monoclonal (14793, CST), sheep anti-CK1α polyclonal (SA527, MRC PPU Reagents & Services) and rabbit anti-ULK1 (8054, CST) primary antibodies were used at a 1:500 dilution. Coverslips were then incubated for 30 min at room temperature with Alexafluor coupled secondary antibodies in blocking buffer and washed an additional three times in blocking buffer. Donkey anti-rabbit IgG Alexa-Fluor 488 (A21206, Thermo Fisher Scientific), goat anti-mouse IgG Alexa-Fluor 594 (A11005, Thermo Fisher Scientific), goat anti-rabbit IgG Alexa-Fluor 594 (A11012, Thermo Fisher Scientific) and donkey anti-sheep IgG Alexa-Fluor 647 (A21448, Thermo Fisher Scientific) secondary antibodies were used at a 1:500 dilution. After submerging in ddH2O, cells were mounted onto glass slides using ProLong gold antifade mountant with DAPI (Life Technologies) and visualised using a DeltaVision system (Applied Precision) and deconvolved using SoftWoRx (Applied Precision). Images were processed using ImageJ and OMERO 5.4.10 software.[77] ImageJ macro quantification of CK1α spindle localisation was performed as previously described.[28,33]

Mass spectrometry

Interactome analysis

For interactome analysis, cells were first lysed in NP-40 lysis buffer. Clarified lysates were incubated with Protein A agarose beads for 1 hr on a rotating wheel at 4°C to pre-clear non-specific binding proteins and filtered through Spin-X columns by centrifugation for 5 min at 13,000 xg. Filtered extracts (5-10 mg protein) were incubated with 10-20 μl of appropriate beads for specified IP for 4 hr at

4°C on a rotating wheel. Following incubation, beads were washed 3x with standard lysis buffer. Bead-bound proteins were denatured and eluted in 2x LDS for 5 min at 95°C. Samples were then filtered through Spin-X columns to remove the beads from the eluate. The filtered eluate was loaded onto a 4-12% Bis-Tris gradient gel and proteins were separated by SDS-PAGE. Gels were stained with InstantBlue and subsequently de-stained in deionised water. A small portion of the eluate was retained for analysis and validation by Western blotting.

To minimise potential protein contaminants, all steps from this point were performed under a laminar flow hood. Disposable scalpels were used to cut protein bands of interest from the InstantBlue stained gels into 1-2 cm cubes, which were subsequently transferred into LoBind 1.5 ml Eppendorf tubes. Gel pieces were washed once in HPLC grade water, and then shrank in anhydrous acetonitrile (ACN) for 5 min with gentle shaking. The ACN was aspirated, and gel pieces were re-swollen with 50 mM Tris-HCl pH 8.0 for 5 min with shaking. The shrinking-swelling process was repeated once more, and the proteins within the gel pieces were reduced with 5 mM DTT in 50 mM Tris-HCl pH 8.0 for 20 min at 65°C. Next, the proteins within the gel pieces were alkylated with 20 mM iodoacetamide (IAA) in 50 mM Tris-HCl pH 8.0 for 20 min at room temperature. Gel pieces were then shrunk again in ACN for 5 min and re-swollen in 50 mM triethylammonium bicarbonate (TEAB) pH 8.0 containing 5 μg/ml trypsin for 16 hr at 30°C for digestion. An equivalent volume of ACN was added to the digest for 15 min with shaking and the supernatant was collected into a fresh LoBind 1.5 ml Eppendorf tube. Gel pieces were then re-swollen with 0.1% (v/v) trifluoroacetic acid (TFA) for 5 min with shaking, and peptides were extracted twice with ACN for 5 min each with shaking. After each extraction, the supernatant was removed and combined with the previous supernatant. The supernatants were then dried by vacuum centrifugation using a SpeedVac.

Digested peptides were reconstituted in HPLC-grade 5% (v/v) ACN containing 0.1% (v/v) formic acid (FA) and injected into a U3000 RSLC (rapid separation liquid chromatography) HPLC chromatography system (Thermo Fisher Scientific) coupled to a linear ion trap-orbitrap hybrid mass spectrometer (Orbitrap Velos Pro, Thermo Fisher Scientific). Peptides were trapped on a nanoViper Trap column (2 cm x 100 μM, C18 5 μM, 100 Å, Thermo Fisher Scientific) and subsequently separated on a 15 cm EasySpray column (Thermo Fisher Scientific) equilibrated with a flow rate of 300 nL/min. Data was acquired in the data-dependent mode, automatically switching between MS1 and MS2 acquisition. Full scan spectra (m/z 400-1,600) were acquired in the orbitrap with resolution set to 60,000 at m/z 400. The 20 most intense ions, above a specified minimum signal threshold of 2,000, were fragmented by collision induced dissociation and recorded in the linear ion trap (full automatic gain control (AGC) target; 30,000, Msn AGC target; 5,000). Raw files were subsequently converted into a list of identified peptides, along with the precursor intensity of the identified peptides, and submitted to the in-house Mascot server (MRC PPU, University of Dundee). Data was searched against the SwissProt human database with variable modifications allowing for oxidation of Met, phosphorylation of Ser/Thr or Tyr residues, along with oxidation or dioxidation modifications. Carbamidomethylation of Cys was set as a fixed modification. Error tolerances were set to 10 ppm (parts per million) for MS1 and 0.6 Da for MS2. Data analysis was performed using Scaffold v 4.4.6 (Proteome Software).

Global proteome and phospho-proteome analysis

Cells were lysed in urea lysis buffer (8 M urea, 20 mM HEPES pH 8.0, supplemented with 1 tablet of cOmplete protease inhibitors per 25 mL lysis buffer and 1 tablet of PhosSTOP phosphatase inhibitors per 10 mL lysis buffer) by Bioruptor® sonication for 15 cycles at 30 sec intervals in LoBind Eppendorf tubes. Lysates were clarified by centrifugation at 13,000 xg for 20 min at 4°C and were then transferred to fresh LoBind Eppendorf tubes. Protein concentration was estimated using the Pierce™ BCA method. Equal protein from each condition were reduced with 5 mM DTT at room temperature for 30 min and alkylated with 20 mM IAA in the dark at room temperature for 15 min. Samples were then digested with Lys-C (1:100) at 30°C for 4 hr. Samples were then diluted with 50 mM TEAB to a urea concentration of 1.5 M and were then digested with trypsin (1:20) at 30°C for 16 hr. The digest was quenched with the addition of 1% FA (v/v) and samples were desalted on 200 mg SepPak C18 cartridges (Waters) and dried by SpeedVac.

Peptides were resuspended in 50 mM TEAB and labelled using tandem mass tag (TMT) labels as per the manufacturer's instructions. TMT labels were resuspended in ACN, added to assigned samples and incubated for 1 hr at room temperature. Following label check by LC-MS/MS, the labelling reaction was quenched with 5% hydroxylamine for 15 min at room temperature. Labelled peptides from each condition were pooled together and dried. Pooled peptides were separated by basic reversed phase (bRP) chromatography fractionation on a C18, 250 x 4.6 mm column, 5 μm, XBridge (Waters, Milford, MA) with Ultimate 3000 HPLC system (Dionex) operating at 500 μL/min with two buffers: buffer A (10 mM ammonium formate, pH 10) and buffer B (80% ACN, 10 mM ammonium formate, pH 10). Peptides were resuspended in 100 μL of buffer A (10 mM ammonium formate, pH10) and separated on a C18 reverse phase column. A total of 96 fractions were collected. 10% of each fraction were concentrated into 24 fractions for proteome analysis, whilst the remaining 90% were concentrated into 12 fractions for IMAC-based phospho-peptide enrichment. Each concentrated fraction was then dried by SpeedVac.

IMAC beads were prepared from Ni-NTA superflow agarose beads that were stripped of Nickel with 100 mM EDTA and incubated in an aqueous solution of 10 mM iron (III) chloride (FeCl3). Dried peptide fractions were reconstituted to a concentration of 0.5 μg/μL in 80% ACN/0.1% TFA. Peptide mixtures were enriched for phosphorylated peptides with 10 μL IMAC beads for 30 min. Enriched IMAC beads were loaded on Empore C18 silica packed stage tips. Stage tips were equilibrated with methanol followed by 50% ACN/0.1% FA then 1% FA. The beads with enriched peptide were loaded onto C18 stage tips and washed with 80% ACN/0.1% TFA. Phosphorylated peptides were eluted from IMAC beads with 500 mM dibasic sodium phosphate, pH 7.0.

Enriched phospho-peptides and peptides were analysed on an Orbitrap Fusion Tribrid mass spectrometer interfaced with Dionex Ultimate 3000 nanoflow liquid chromatography system. Peptides were separated on an analytical column (75 μm x 50 cm, RSLC C18) at a flow rate of 300 nL/min using a step gradient of 5-7% solvent B (90% ACN/0.1% FA) for the first 10 min, followed by 7-35% up to 150 min. The total run time was set to 180 min. The mass spectrometer was operated in a data-dependent acquisition mode. A survey

full scan MS (from m/z 375-1500) was acquired in the Orbitrap at a resolution of 120,000 at 200 m/z. The AGC target for MS1 was set as standard and ion filling time set at 50 ms. The most intense ions with charge state ≥ 2 were isolated and fragmented using higher collision dissociation (HCD) fragmentation with 38% normalised collision energy and detected at a mass resolution of 50,000 at 200 m/z. The AGC target for MS2 was set as standard and ion filling time set at 86 ms, while dynamic exclusion was set for 60 s.

The mass spectrometry raw data were searched using Sequest HT search engines with Proteome Discoverer 2.1 (Thermo Fisher Scientific). Phosphopeptide-enriched fractions from each replicate were searched against the Uniprot protein database. The search parameter used were carbamidomethylation of cysteine residues and TMT of lysine and N terminal as a fixed modification. Oxidation of methionine, the phosphorylations of serine, threonine and tyrosine, were selected as dynamic modifications. Trypsin was set as the protease and a maximum of two missed cleavages were allowed. Precursor mass tolerance was set to 10 ppm, and a fragment mass tolerance of 0.02 Da was allowed. All peptide-spectrum matches (PSM) were identified at a 1% false-discovery rate (FDR). The probability of phosphorylation for each site was calculated by the phosphoRS node in Proteome Discoverer.

QUANTIFICATION AND STATISTICAL ANALYSIS

Statistical analysis was determined using unpaired Student's *t*-test for single comparisons and for multiple treatments analysis of variance was performed followed by the post-hoc tests described in figure legends using Prism® Version 8.0.